Engineering Structures 307 (2024) 117812

Contents lists available at ScienceDirect

Engineering Structures

journal homepage: www.elsevier.com/locate/engstruct

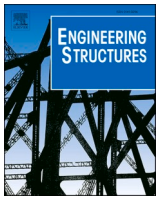

Fatigue assessment of historic retrofitted through-truss riveted railway bridge

Camila Parodi-Figueroa [a,b,*], Dina D'Ayala [a], Wendel Sebastian [a]

[a] Department of Civil, Environmental and Geomatic Engineering, University College London, London, UK
[b] Departamento de Obras Civiles, Universidad de La Frontera, Temuco, Chile

A B S T R A C T

Fatigue damage has been the most common reason for failure in riveted bridges, with the stringer-to-floor-beams connections being identified as the most prone-fatigue locations by several studies. When assessing fatigue damage of historic riveted railway bridges, the analysis usually considers the structure in its current configuration, disregarding any retrofitting the bridge has experienced during its lifetime. This paper presents a fatigue analysis of a one-century-old riveted through-truss railway bridge, part of the Chilean North-South railway line, considering all interventions made to the superstructure since its construction. To perform the analysis, a detailed train loading spectrum is defined considering historical and current data of freight trains and traffic to generate a realistic loading model for the bridge. FE models are generated for the bridge in all configurations (initial and after each retrofitting), and the fatigue damage is evaluated through S-N curves from the Eurocode. The accumulated fatigue damage obtained by this sequence is then compared with a fatigue analysis of the structure in its current configuration. The comparison shows that the fatigue damage is significantly underestimated when assessing the bridge considering only its current configuration and that the retrofitting can substantially change the structural response at the stringer-to-floor beam connections.

1. Introduction

As the railway infrastructure ages, with more than a third of steel railway bridges being more than 100 years old [1,2], fatigue has been increasingly studied over the last decade. Several studies, including the European project Sustainable Bridges [1], have identified fatigue as the most common cause of failure in metal bridges, whether triggered by corrosion, increased traffic loads, bridge age and condition [3]. Moreover, according to a report by Kühn et al. [4], railway bridges are among the structures more often damaged by fatigue.

Fatigue assessment of railway bridges is usually associated with high cycle fatigue, indicating that failure may occur at stress levels lower than the yield strength of the material when the structure is subjected to a large number of cycles [5]. Bridges exposed to high cycle fatigue are mostly assessed through one of two approaches: the *Nominal Stress* approach (also known as S-N), which considers the effects of mean stresses and stress concentrations, or *Fracture Mechanics*, based on crack propagation theory [6].

The Sustainable Bridges European project [1] indicated that, for historic open deck riveted truss bridges, fatigue problems usually start in the transverse structure since these short elements have to endure more stress cycles than the main girder's components. This observation is validated by more recent studies [7,8], which have identified riveted stringer-to-floor-beams and floor-beams-to-truss-girder connections on historic riveted railway bridges as the components most prone to fatigue failure. These connections, shown in Fig. 1 for a historic riveted bridge in Chile, are usually made of double-angle riveted joints between members designed as shear connections only. However, given the high number of rivets usually associated with these connections, there is some degree of rotational stiffness, which generates a state of flexure and shear within the members (see Fig. 2). Previous studies have identified two mechanisms that cause deformation-induced fatigue due to secondary effects in these connections [8,9]:

1.1. Rotation of stringer ends due to bending

The connection restrains the end rotation of the stringer, which in turn produces tensile stresses in the connecting members. If the stringer is stiff compared with the floor beam, then the bottom of the connections are in tension (Fig. 2(a)), while if the relative stiffness of the floor beam compared to that of the stringer is high (Fig. 2(b)), then the negative bending results in tension at the top of the connections.

1.2. Interaction between the main truss girder and the floor system

The global flexural deflection on the main truss girder causes the longitudinal displacement of the floor beams connected to the bottom

* Corresponding author at: Department of Civil, Environmental and Geomatic Engineering, University College London, London, UK.
E-mail address: camila.parodi@ufrontera.cl (C. Parodi-Figueroa).

https://doi.org/10.1016/j.engstruct.2024.117812
Received 23 August 2023; Received in revised form 12 January 2024; Accepted 4 March 2024
Available online 21 March 2024

Nomenclature

L	Bridge span (m).
σ_x	Direct stresses associated with the longitudinal axis of the structural member (MPa).
σ_y	Direct stresses associated with the transversal axis of the structural member (Mpa).
σ_1	Maximum tensile principal stress determined by Mohr Circle equations.
τ_{max}	Maximum shear stress (MPa).
S_e	Endurance limit of S-N curve (MPa).
σ_a	Stress range (MPa).
N_i	total number of cycles that the connection can endure at a determined stress range.
σ_c	reference value of the fatigue strength at N_c= 2 million cycles (MPa).
σ_D	fatigue limit for constant amplitude stress ranges at the number of cycles N_D (MPa).
DI	Accumulated fatigue damage index.
n_i	number of cycles with stress range greater than the endurance limit of the S-N curve, (i represents each $\sigma_a > S_e$ for the specific stringer-to-floor-beam connection).
t_j	annual frequency of train j.
y_j	number of years during which train j has been in operation.
T_y	train year.
NAL	Number of locomotives times locomotive's weight.
t_L	wagon's tare load (t).
$\overline{f_w}$	mean annual freight load per wagon (t).
$C_{w\%}$	percentage of wagon's capacity.
C_w	load capacity per wagon (t).
w_L	wagon's axle load (t).
n_w	number of wagons.
f_t	freight load per travel (t).
f_{by}	annual freight load over bridge A (t).
$\%f_{Ly}$	percentage of total annual freight load in the Chilean railway network (t).
f_b	mean annual freight load for the period (t).
f_L	mean annual freight load in the Chilean railway network (t).
F	train annual frequency.

chord in through-truss bridges. This deformation is partially restrained in the floor beams due to the axial stiffness of the stringers and the connections between them. In turn, the floor beams could experience additional bending around the weak axis.

As Fig. 1(b) shows, the floor beam is generally restrained to rotation by the truss girder, and considering that the truss girder is stiffer than the floor beams, this connection directly affects the stress distribution along the floor system.

Most literature that assess fatigue in historic metallic railway bridges considers fully fixed stringer-to-floor-beams and truss-girder-to-floor-beam connections, assuming, that this is a conservative, and therefore safe approximation of the real rotational stiffness between members [5,10–12]. Members within the truss girder of these bridges have also been modelled has fully-fixed connections, and even riveted joints in old metallic lattice girders have been observed to exhibit a rigid behaviour regarding out-of-plane rotation [13].

To reduce computational effort, many studies use global FE numerical bridge models with frame elements [7,10,14]. Better results are shown through the use of shell elements [15], as they provide a more accurate stiffness distribution. Nonetheless, global models of riveted bridges do not consider the details of the riveted double-angle connections usually found in these historic bridges. Thus, the stress response does not contemplate the effect of the rivet holes and rivet clamping action within the connection's area. To avoid underestimating the stress response due to train traffic, the use of a Stress Concentration Factor (*SCF*) has been introduced to increase the value of the computed stress around the rivet hole [16]. Imam et al. [15] analysed a double-lap joint through an advanced numerical FE model in *ABAQUS*, and determined the *SCF* in different positions around the edge of the rivet hole, to compare with the experimental results by Carter [16]. The results were later validated by Marques [14] with an advanced numerical FE model in *ANSYS*, who concluded, that the maximum *SCF* is around the rivet hole of the central plate at the interface between the other plates. Marques et al. [17] also determined an *SCF* through a global-local FE model of floor-beam-to-cross-girder connections in a riveted bridge. The *SCF* was calculated on the gusset plate connecting the floor beam's top flange with the girder's upper structural members. The results showed that as clamping stress increases, the *SCF* decreases and eventually reaches a value of around 1.0, where it stabilises.

Unlike historic buildings, where historic fabric preservation usually

(a) (b)

Fig. 1. Typical riveted double-angle connections in Chilean railway bridges. (a): Stringer-to-floor-beam connections; (b): Floor-beam-to-truss-girder connection.

controls the design when rehabilitating works are needed [18,19], historic railway infrastructure is retrofitted considering their functionality to current loading conditions. These aging structures, many of which were built more than 100 years ago, have been exposed through time to axle load of greater magnitude than the ones they were originally designed for. Such loads might have induced fatigue damage to the superstructure over time [20,21]. To improve the live load-carrying capacity of these bridges and adapt their design to environmental loading conditions, such as wind and earthquake, different retrofitting solutions have been applied worldwide. The most common retrofitting technique for historic truss bridges involves adding locally more material (plates) to the more stressed members to enhance their load-carrying capacity [10,11,22]. Other retrofitting methods, aimed at a more global improvement of the structure, comprise replacing gusset plates and aged rivets to improve connection performance; adding new members (such as cross girders) or external prestressing of the truss to improve shear and bending capacity [22–25]. Less common methods include: superimposing a steel arch to a truss bridge to improve global bending capacity [26,27]; adding a lower arch or a new truss; or adding a beam between existing main truss girders for the same purpose [23,24]. These retrofitting solutions have improved historic steel bridges' capacity and structural response, and have allowed their continuous use. Most of these solutions are discussed as specific case studies, while only few publications present a compendium of retrofitting measures that could be used as a general guide to strengthen historic steel bridges. Tapia's research on Chilean railway bridges [20] stands out among these studies because it displays several retrofitting techniques used in historic truss bridges. Moreover, the timing and sequence of retrofitting interventions on a railway bridge should also be considered, as these can change significantly the bridge's structural response, and hence invalidate any fatigue damage analysis. Still, most studies assessing fatigue damage in historic riveted railway bridges focus on the structure's current configuration [10,11,28,29], as original drawings are usually unavailable.

A recent study [30] shows the importance of accurately representing historic trains in the loading spectra when evaluating fatigue damage. However, given the lack of historic data, past traffic on historic bridges is usually assumed and very few studies have considered the actual variations of train loading [30]. Alternatively, loading models are used, such as the one presented by Akesson [31], where train loading is estimated based on the freight tonnage statistical data, considering the variation of train layouts and axle spacings, or the past traffic model suggested by the International Union of Railways [32], which represent the past traffic through typical trains during different periods.

For fatigue analysis of historic bridges, the assumption that current train loadings have been applied since the bridge's construction date it is very conservative [30].

To address some of the shortcomings identified in current literature, this study focuses on the fatigue assessment of a historic Chilean steel riveted truss bridge, Bridge A, considering the actual sequence of different retrofitting interventions which have been applied to the superstructure since its construction date. The fatigue analysis contemplates a sequence of train loading selected according to historic data from the Chilean Railway Company and other historic sources. As most literature identifies stringer-to-floor-beam connections as the locations that are most prone to initiate fatigue damage in riveted railway bridges [1,7,8,33], the fatigue analysis will be focused on these locations. The methodology applied follows Iman's [5] by using the S-N Curves of Category Detail 63 and 71 provided by Eurocode 3 (EC3) [34], which have been recommended by several researchers [35,36], and a total fatigue damage index for each stringer-to-floor-beam connection is calculated by applying Miner's rule [37]. The fatigue damage is then compared with the damage obtained by assessing the bridge in its current configurations omitting the changes that the structure has endured in its lifetime, as it is common in most case studies. This comparison allows to demonstrate how the total fatigue damage is influenced by the bridge strengthening, and why the sequence of strengthening its critical to the bridge current performance.

2. Methodology

The research objectives are to identify how both loading history and retrofitting history of Bridge A influence the variation of location in time of the connections most affected by fatigue and the magnitude of the residual fatigue life that these connections can endure.

The loading spectrum is defined according to the information available and given by the Chilean railway company by following the process shown in the upper part of Fig. 3. Most data was defined following factual information, although some had to be determined through extrapolation using linear or exponential trends. The number of travels per each year was determined by integrating real data with best fit curves.

Fatigue in this study is assessed through the S-N approach as described in EC3 [34] and Imam [5], focusing on the principal tensile stress response of the stringer-to-floor-beam connection, considering a general surface cracking due to a pre-existing condition around the rivet hole area as mode of fatigue failure [34,38].

In agreement with Imam and Salter [30], the loading spectra for this study is consistent with trains and traffic that have transited through Bridge A during different stages. To consider the succession of all structural retrofitting applied to the bridge in time, several numerical models are created to represent each different structural configuration since its construction date. Then, specific loading spectra are applied to each corresponding historic configuration and all the steps shown in Fig. 3 are performed for each model.

Significant stress responses are obtained for the stringers-to-floor-beams connections. This response is amplified considering two phenomena: the stress concentration around the rivet holes (accounted by *SCF*) and the dynamic effect of the train impact over the bridge and track irregularities, accounted through the Dynamic Amplification Factor (*DAF*). The *SCF* is determined by the relationship between clamping stress and *SCF* given by Marques et al. [17], assuming a clamping stress equal to 80% of the yield stress, as proposed by Wilson and Thomas [39]. The *DAF* is determined using Eq. (1) [40]:

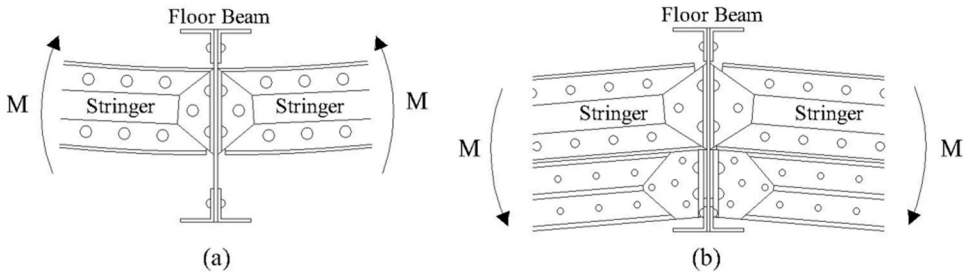

Fig. 2. Tensile stress in the connections due to bending: (a): Low stiffness of the floor beam compared to the stringers; (b): High stiffness of the floor beam compared to the stringers.

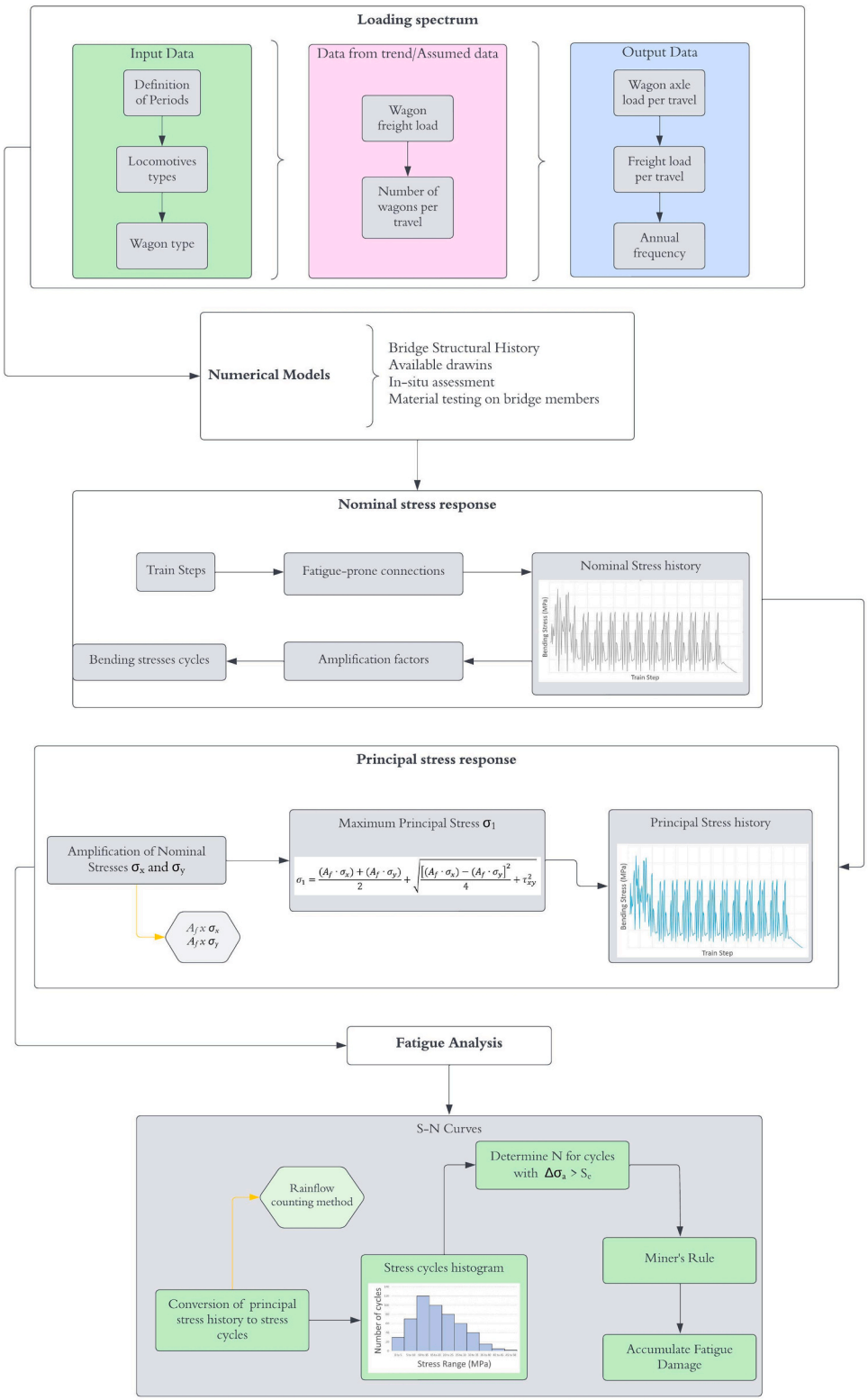

Fig. 3. Methodology to determine fatigue damage.

$$DAF = 1.19 + \frac{21}{L + 46} \quad (1)$$

Both factors are then used to amplify the stress response in the connection by the amplification factor A_f, as shown by Eq. (2).

$$A_f = SCF \bullet DAF \quad (2)$$

As the stringer-to-floor-beam connections are subject to both bending and shear stresses, this study uses maximum tensile principal stress (σ_1) history to determine the stress ranges contributing to fatigue. Direct stresses, σ_x and σ_y, are amplified by A_f, and σ_1 is determined by applying Mohr Circle equations, as shown in Fig. 3.

The σ_1 response is filtered to simplify it and determine relevant stress ranges (σ_a). The filtering process discretises the response by omitting

minor stress variations, i.e. by eliminating small oscillation of stress value that are not significant to the fatigue damage. In this way the cycles are linearized by considering only the maximum and minimum values of the response for each cycle.

The filtered response is analysed by applying the rainflow counting method. To this end, a Matlab routine is created [41], as shown in Fig. 4, to count all σ_a of closed cycles and process the stress histogram to display the number of cycles (N_i) whose range is between a determined value, usually multiples of 5 or 10 MPa, as shown in Fig. 3.

Once σ_a of closed cycles are determined, S-N curves are used to determine which ranges are subjected to fatigue damage by comparing σ_a with the S-N endurance limit (S_e). The literature review highlighted that the EC3 S-N curve category detail 71 [34] provides a realistic endurance limit to assess fatigue damage, according to experimental tests on riveted bridges [36]. On the other hand, Cremona et al. [35] and SB-LRA [1] recommends considering the category detail 63 [34] as a

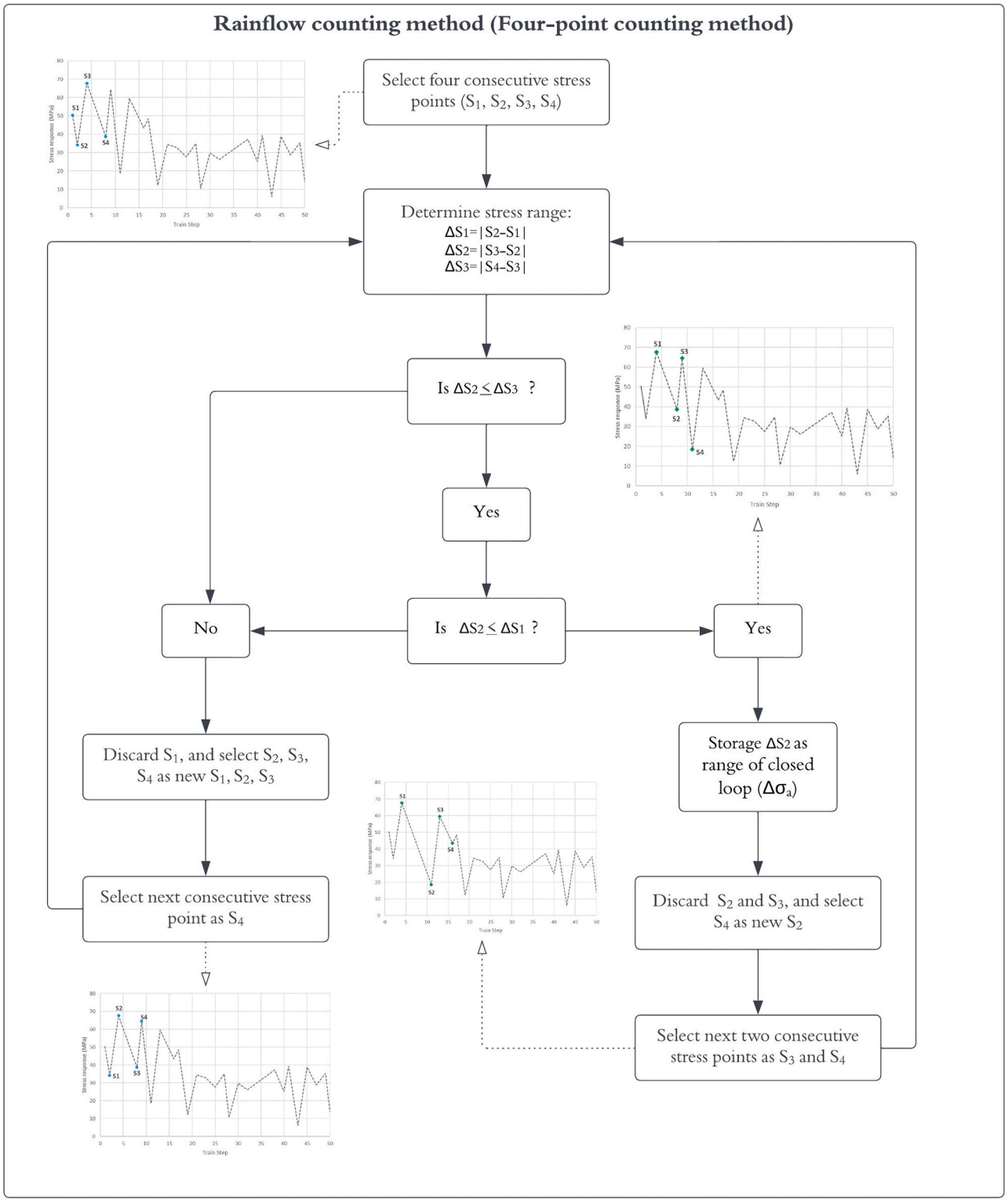

Fig. 4. Matlab routine to process stress range of closed cycles with the rainflow counting method.

more conservative choice. As Bridge A was designed and built by a French company, both S-N curves, shown in Fig. 5, are selected to assess fatigue damage.

Eq. (3) [34], is used to determine N_i for each σ_a greater than S_e.

$$N_i = \begin{cases} \dfrac{\sigma_c^3 \bullet 2 \bullet 10^6}{\sigma_a^3} & if \quad \sigma_a > \sigma_D \\ \dfrac{\sigma_D^5 \bullet 5 \bullet 10^6}{\sigma_a^5} & if \quad \sigma_D \geq \sigma_a > S_e \end{cases} \tag{3}$$

The accumulated fatigue damage index (*DI*) is determined by the Palmgren-Miner rule [37], using Eq. (4). *DI* is determined for each stringer-to-floor-beam connection considering the train traffic defined by the loading spectra for each numerical model representing the bridge in a different configuration.

$$DI = \sum t_j \bullet y_j \left(\frac{n_i}{N_i}\right) \leq 1 \tag{4}$$

3. Chilean railway infrastructure

The railway infrastructure started to be implemented in Chile by the mid-1800 s Fig. 6 shows the freight loads used in the Chilean railway infrastructure from 1890 to 2021. Historical freight data from 1890 to 1959 are taken from archives summaries from the Chilean Railway Company, EFE [42–64], Nunez [65], and Marin [66,67], complemented up to 1973 with information taken from León [68]. Data on freight load from 1980–1996 is estimated based on the information given by Cabrera [69], and the data for the period 2000–2021 is taken from the annual summaries of EFE [70–86].

Nowadays, Chile has a railway network of approximately 2400 km [87], which can be described as a main north-south route from Valparaiso to Puerto Montt, with several east -west branches.

Most of the main railway line from Santiago to the south is 5'6" gauge, including the railroad where the case study is located. Other areas of the railway network, such as part of the North, Arica and smaller branches in the South, have narrower gauges.

The Chilean railway network has more than 300 bridges with a span length exceeding 11 m [88]. Of these, many are located in the central and south regions of the country and were built in the late 19th or early 20th century, with structures made of mild steel [20,88]. Most of these bridges are still in use, and fatigue assessments concerning their current structural health conditions have not been carried out. Therefore, it is not possible to establish their remaining life considering current train loads.

Because trains have increased their loading over time [20], retrofitting solutions were applied to many Chilean bridges to improve their live load-carrying capacity and adapt their design to other loading conditions.

Tapia's [20] unique and comprehensive study allows identifying typical truss railway bridges in Chile and determining the changes in structural configuration that they underwent during their lives. According to Tapia [20] two truss typologies are particularly common on the Chilean network: the rectangular Howe with double-cross diagonals and Town Lattice with or without vertical members.

Most historic Chilean riveted railway bridges were designed and built by the French Company Schneider at Le Creusot [20]. As described by Tapia [20], Chilean steel truss railway bridges built between the end of the 19th century and the beginning of the 20th century are similar to those described in European and American studies: member sections are made of a combination of riveted plates and angles with riveted connections made with Gusset plates. Structures are commonly open deck truss bridges with no ballast, as early railway features described by Hayward [89], and there are various through and deck-truss bridges.

Chilean Design Standard for railway bridges [40,90,91] indicates a density of 78.5 kN/m^3 for early steel bridges, slightly higher than the recommended values for European Bridges [1,35]. In addition, a Young's Modulus of 210 GPa is established, which concurred with other studies that assessed fatigue in historic steel railway bridges [10,11], and a Shear Modulus of 77 GPa, that is consistent with the recommended value for the assessment of historic steel European railway bridges [1].

According to Tapia [20], the material used in early Chilean railway bridges is described as metal with yield strength limits between 280 and 340 MPa, and ultimate limits between 380 and 450 MPa based on material testing. Although there is no detail on whether this metal refers to cast iron, wrought iron or mild steel, *EFE* recommends using mild steel properties for historic metal railway bridges when assessing them [40,91]. Furthermore, yield and ultimate strength values provided by Tapia are consistent with steel strength values used in historic European railway bridges, as shown in Table 1.

Nonetheless, it should be considered that Tapia provided these material strength values in his book published in 1945, for structures that have been in use for more than 75 years to the present time, hence mechanical characteristics might have degraded due to a variety of phenomena.

The Chilean Design Standard for railway bridges [40,91] establishes a yield strength of 220 MPa to assess historic steel railway bridges. However, material testing of early steel bridges in Chile shows

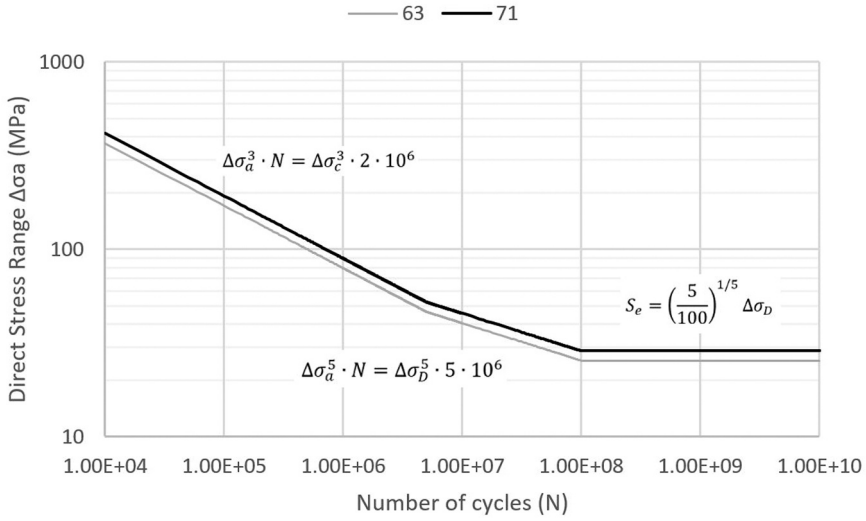

Fig. 5. EC3 Fatigue S-N Curve Category Detail 63 & 71.

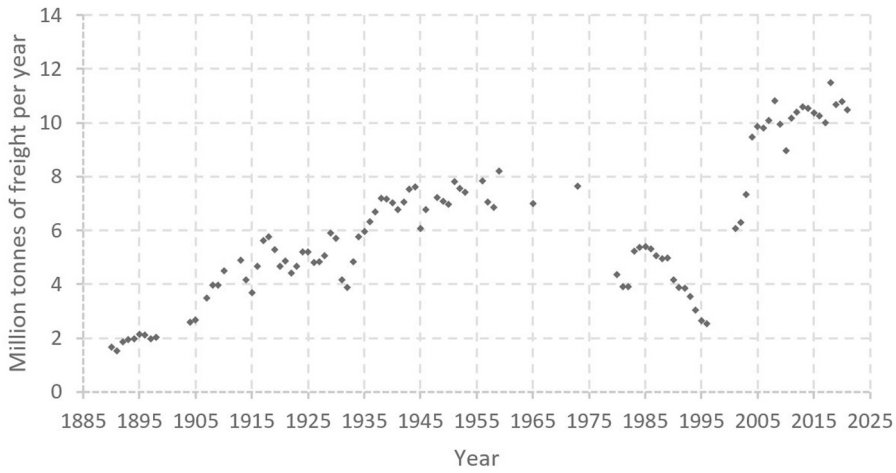

Fig. 6. Yearly Chilean railway freight traffic.

Table 1
Structural steel properties for railway bridges in different countries, based on material testing.

Source	Country	Chilean Steel Grade	f_y [MPa] (min)	f_u [MPa] (min)	f_u [MPa] (max)
EFE, 2002; NCh 203, 2005[40,92]	Chile	A37-24ES	240	360	460
Tapia, 1945 [20]	Chile	-	280	380	450
Cremona et al., 2013[35]	Several European countries	-	261	320	380
Ermopoulos and Spyrakos, 2006[11]	Greece	-	280	308	-
Larsson, 2009 [93]	Sweden	-	231	359	522
Larsson, 2009 [93]	Germany	-	224	304	578
Höhler, 2005 [94]	Germany - France	-	217	343	578

admissible tension similar to or greater than steel A37–24ES [95], the lowest grade structural steel used in Chile, whose mechanical properties are summarised in Table 1.

4. Description of Bridge A

The chosen bridge for this study, Bridge A, is a Howe single-span through-truss bridge with an open deck built in 1895 and retrofitted in 1927, 1935 and 2021, with structural drawings for each retrofitting being available. The bridge's main truss parallel girders are made of ten panels of double diagonals Howe truss 15.3 m long and 1.45 high, as shown in Fig. 7(a). The girders are 4.55 m apart and connected at the bottom chord through transverse floor beams, a horizontal bracing system every two panels and longitudinal stringers, as shown in Fig. 7 (b). The superstructure is simply supported through fixed knuckle pins and four-roller expansion bearings at each end of the truss girders.

Bridge members comprise built-up cross-sections with a combination of different plates and angles, as shown in Fig. 8. Connections between floor beams and stringers, and floor beams and bottom chord are through double angles, as shown in Fig. 9.

The bridge has experienced three retrofitting since its construction. The first retrofitting was applied in 1927 and was mainly implemented because of the high stresses the original stringers experienced with the increasing train axle loads. An I-cross section was added below the stringers to increase their moment of inertia, as shown in Fig. 9. Additional horizontal plates were added to the upper and lower flange of the central portion of the floor beams, away from the supports, as shown in Fig. 10, where "FB2" refers to the beam retrofitting. This retrofitting increased the strength of the floor system and allowed for heavier trains to transit the bridge.

In 1935 the bridge experienced the second retrofitting to reduce deflections at mid-span caused by increasing train loads. As shown in Fig. 11(b) and (c), horizontal plates were added to bottom and top chords' flanges to increase their stiffness. Fig. 11(d) shows that the diagonals were also retrofitted to avoid buckling. These interventions appear complementary to the first strengthening project, and might have been conceived then, to increase the global bridge stiffness. However, they were probably delayed to financial restrictions.

Finally, in 2021, as part of the programme "*Chile on Rails*" [99,100], the bridge underwent a new strengthening to ensure its safe use and maintenance. The top and bottom chords and the diagonals were strengthened by adding plate to the flanges, while angle profiles were added to the floor beams, as shown in Fig. 12. Besides providing additional stiffness, to limit defections caused by current trains, this intervention reduces stress concentration levels caused by the strengthening of 1927, which produced an abrupt reduction of the floor beam cross-section at the ends of the members connected to the bottom chord girders.

To account for these modifications in time of the bridge structure, four distinct numerical FE models are developed for the fatigue analysis and subjected to the relevant progression of train loading.

5. Loading spectrum

Live loads, representing freight and passenger trains, are an essential input for the fatigue assessment of railway bridges. For this study, the choice is made to consider the freight traffic only, as representative trains loading, due to the following considerations: (i) freight trains usually have heavier locomotives, (ii) the number of wagons used to move freight load is greater than the ones used in passenger travels, therefore generating more stress cycles that can contribute to fatigue damage, and (iii) in the last two decades, only freight load trains have transited over the bridge, as passenger traffic was suspended since 2007 [99].

The definition of the loading spectra has required an extensive research of historic and current data on trains used in the Chilean railway network [20,42–64,70–86,101–121]. The annual freight tonnage shown in Fig. 6 is used to define the wagon loads and the representative trains are defined following historic records of real trains employed on

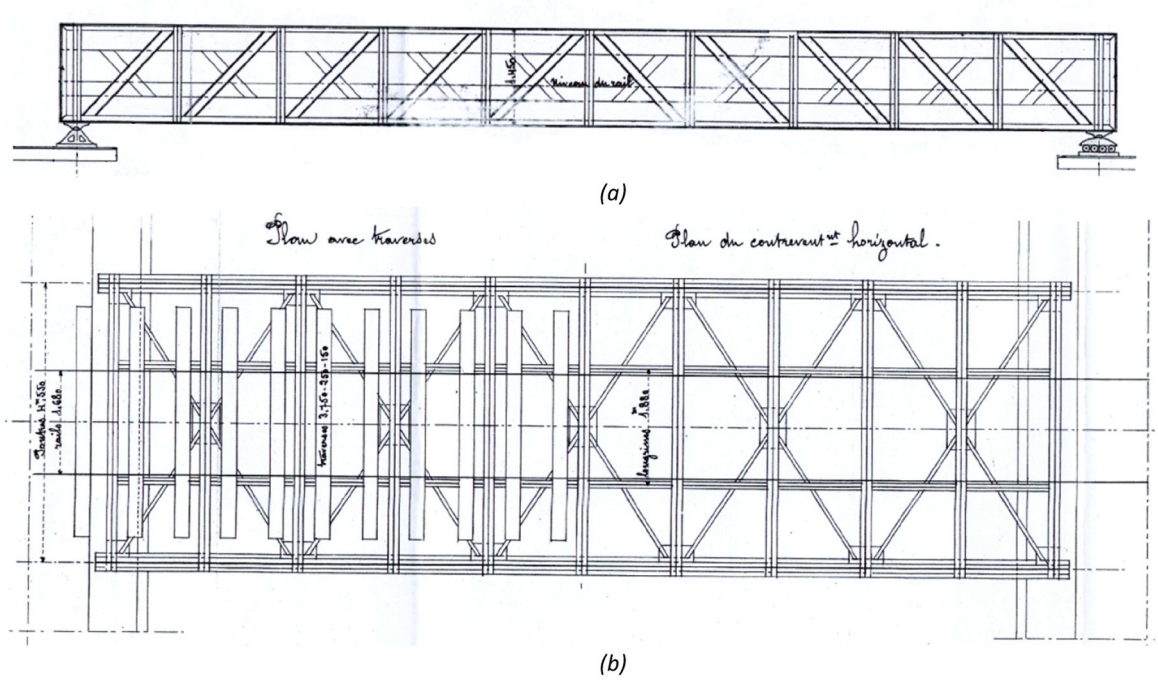

Fig. 7. Originals drawings for the bridge from Le Creusot Company, EFE [96] (a): Main truss girder (b): Bridge transversal bracing system.

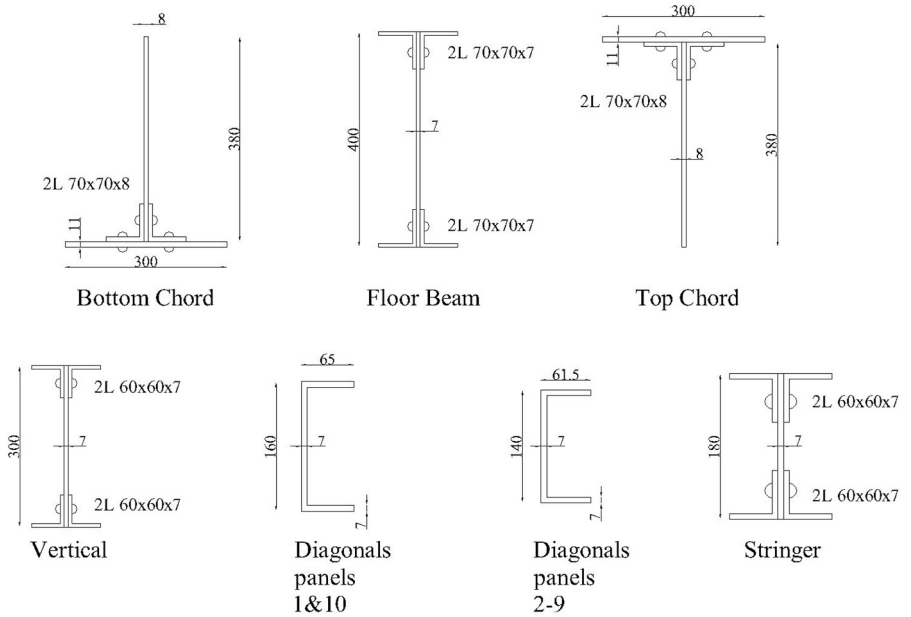

Fig. 8. Member's cross-sections of Bridge A. Measurements are in mm. Rivets of 20 mm are used to connect plates and angles, with a separation of 60 mm in the longitudinal direction. Original drawing from EFE [96], redrawn by the authors.

the Chilean network, for which evidence is available that they transited over Bridge A. The selection process is made by identifying first the period of use and number of units for various locomotives models, then the composition of the trains in terms of typology and number of wagons and wagon's axle loads, and finally the train's frequency F of transits over the bridge.

5.1. Periods of use and characteristics of locomotives

Coombs [102,103] compiled a database of all locomotives acquired by *EFE* from 1855 to 1953 that includes the locomotive's company and name, axles' layout, purchase year, number of locomotives and train type according to *EFE's* classification (consecutive numbers between 1 and 110). Locomotives and tender characteristics can also be found in Tapia [20] for the heaviest types between 1903 and 1945, while Thomson [101] provides load values for locomotives and tenders for all locomotive types defined by *EFE*, together with various historic details about the use of locomotives in the south of the country, where Bridge A is located. Simms [122,123] lists the locomotives typical of freight trains in south Chile in recent years.

From 1885 until 1953, when the last steam locomotives were purchased by *EFE*, information about number of acquired locomotives and their details, is very robust. Therefore, the correlation between most representative locomotives and their period of use, is reliable up to this

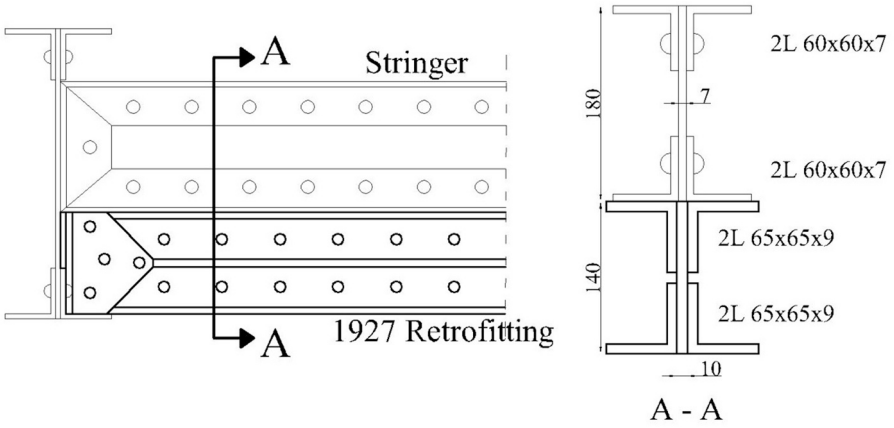

Fig. 9. Retrofitting of Bridge A stringers in 1927. Rivets of 17 mm with a separation of 51 mm are used for the retrofitting of stringers. Original drawing from EFE [97], redrawn by the authors.

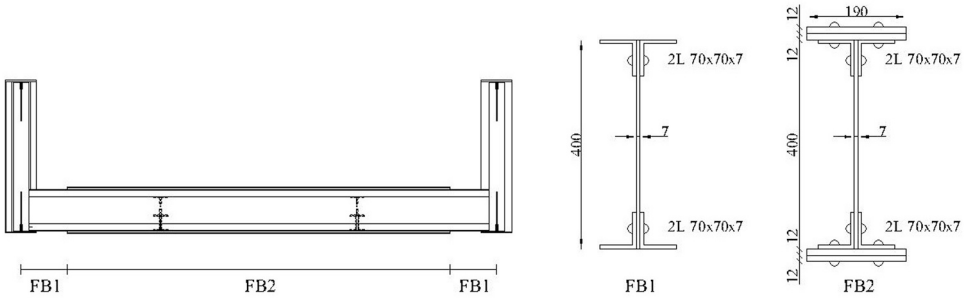

Fig. 10. Retrofitting of Bridge A floor beams in 1927. Rivets of 20 mm with a separation of 60 mm are used for the retrofitting of floor beams. Original drawing from EFE [97], redrawn by the authors.

date. However, after 1953, technical details of electric and diesel locomotives in use or dismissed at the time, as well as the type and number of yearly new purchases, are much less consistent. Most of the information from this last period is obtained from *EFE* [62–64,70–86], Sommers [124], Simms [122,123], and annual summaries from *Fepasa* [105–121], but the level of detail is inferior to the ones compiled by *EFE* before 1959, or the extensive accounts that can be found in Thomson [101] and Coombs [102,103].

Steam locomotives fell out of use after the 1960 s, as electric and diesel locomotives slowly replaced them. However, as Fig. 13 shows, the total number of locomotives yearly in use by 1990 were down approximately 40% compared with 1975, mainly due to reduced rate of acquisition of new locomotives in comparison to the number of steam engines retired [101]. In 2021, the company *Fepasa,* which now carries most freight to the country's south, where Bridge A is located, owned 50 locomotives in use on the railway network, of which 47 are broad gauge [121].

Fig. 13 shows that the number of freight wagons per year has also been significantly reduced since the 1970 s. However, as seen in Fig. 14, the number of freight wagons has not influenced much the overall travel capacity for tonne of freight, as nowadays the wagons are used more efficiently and trains travel greater distances.

Based on the previously described information, the maximum axle load for locomotives used on the Chilean railway network between 1883 and 1994 shows an overall increasing trend (Fig. 15). For the period between 1895 and 1904, the increase of locomotives weight was modest, with a variation of approximately 12 tonnes between models (29% variation). Thus, this period can be represented by a single locomotive type. Between the 1900 s and 1940 s a rapid growth of locomotive axle load can be observed well represented by a linear trend. Therefore, this period is subdivided in several interval identified by the acquisition of new heavier locomotives, as recorded by Tapia [20]. The locomotives with highest weight are recorded in use in the period 1936 to 1940 (Fig. 15), however these were not in transit on the branch of the network where Bridge A is located and therefore are disregarded in the present study. For the four decades between 1940 and 1980, there is modest information and little variation in the weight of locomotives. Therefore, the period is divided in four decades, to each of which corresponds one locomotive model. There is also limited information about the locomotives acquired by *EFE* between 1981 and 1993. Given the low freight traffic during this period (Fig. 6), it is assumed that the two models of diesel machines D-2300 s which were being purchased since the earlier 70 s were primarily used.

From 1994, the company *Fepasa* took charge of most of the freight load. From their annual summaries from 2004 to 2021, it can be inferred that there is low variation in the type of locomotives used in the last two decades [105–121]. As shown Table 2, up to four locomotives types are used to distribute freight load in the broad-gauge railway network. The heaviest diesel locomotives D-3300 purchased from 2012 onward, account for only 7% of the dispatched freight load. The two most used locomotive types, D-2300 and D-1800, were already in stock in 1998, therefore a single period from 1994 to 2013 is identified, characterised by these two locomotives with their occurrence as recorded for the year 2004, in Table 2. The final period from 2014 to 2022, includes also the diesel locomotive D-3300 acquired in 2012 (see Table 2).

The considerations outlined above have been automated in a Matlab routine which couples the appropriate locomotives loads and axles characteristics to each of the above periods, as summarised in Fig. 16. Specifically, the locomotive's model selection criterion, for each period, is the highest product of the number of each model in service in the period multiplied by its weight (*NAL*), not necessarily resulting in choosing the heaviest locomotive. From 1981 less technical information

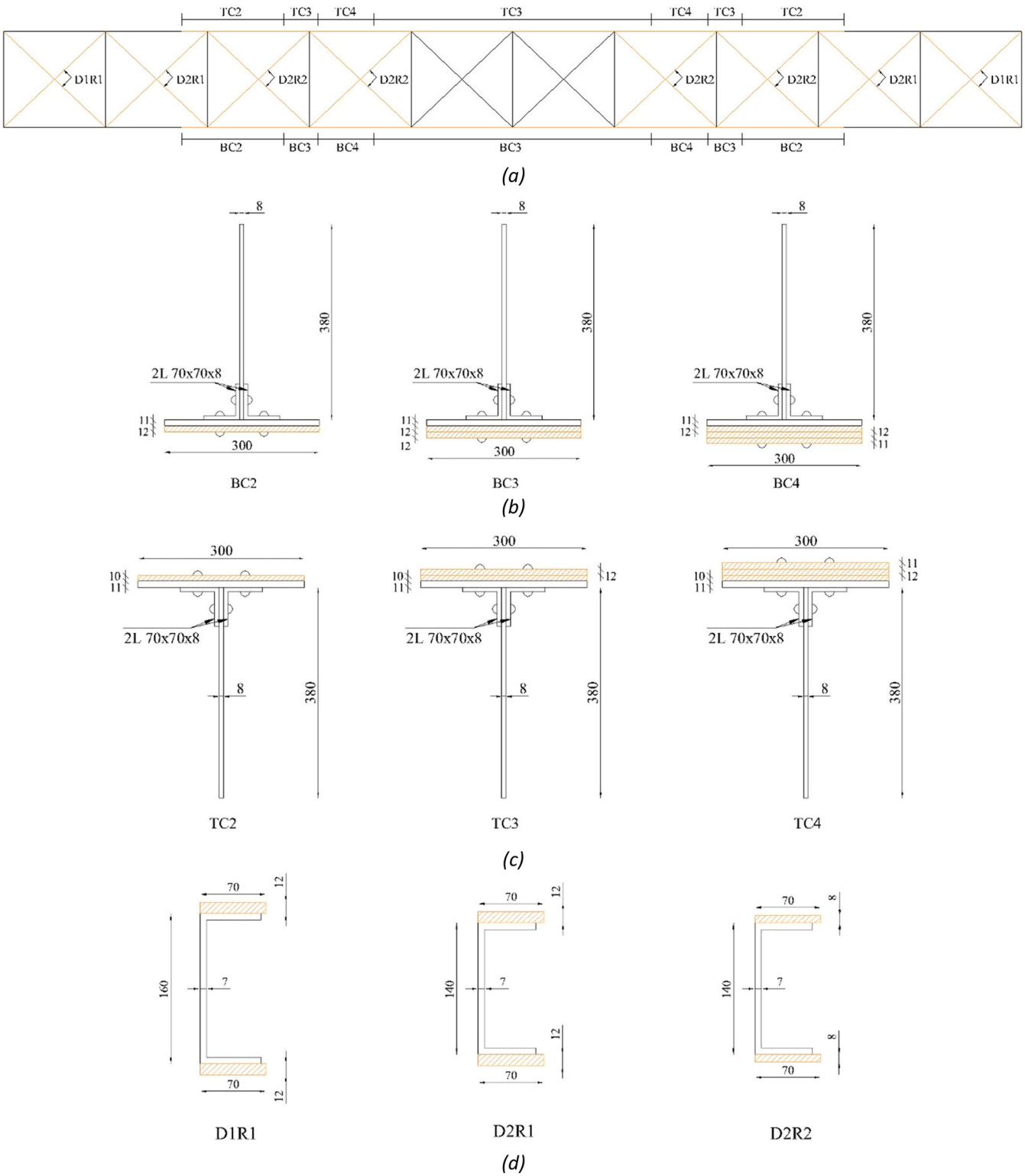

Fig. 11. Retrofitting of Bridge A in 1935. Rivets of 20 mm with a separation of 60 mm are used for this retrofitting. Original drawing from EFE [98], redrawn by the authors (a): Bridge longitudinal view with retrofitting outlined in orange (b) retrofitting of truss' bottom chords (c) retrofitting of truss' top chords (d) retrofitting of truss' diagonals.

is available regarding locomotives purchased by *EFE*, thus, the sum of the most common models are used.

5.2. Wagon type and wagon axle load

For each of the periods identified in Section 5.1 (Fig. 16), the choice of wagon's model and number of them forming the train, is based on the historic information presented in the annual summaries of *EFE* [42–64], Tapia's work [20], Marin [66,67], Nunez [65], and the manual of wagons of *EFE* [125]. Different types of 4-axle wagons are selected for each period with different tare loads (t_L), ranging between 12 and 18 tonnes. These mainly represent "*flat wagons*" with capacity of 30 tonnes

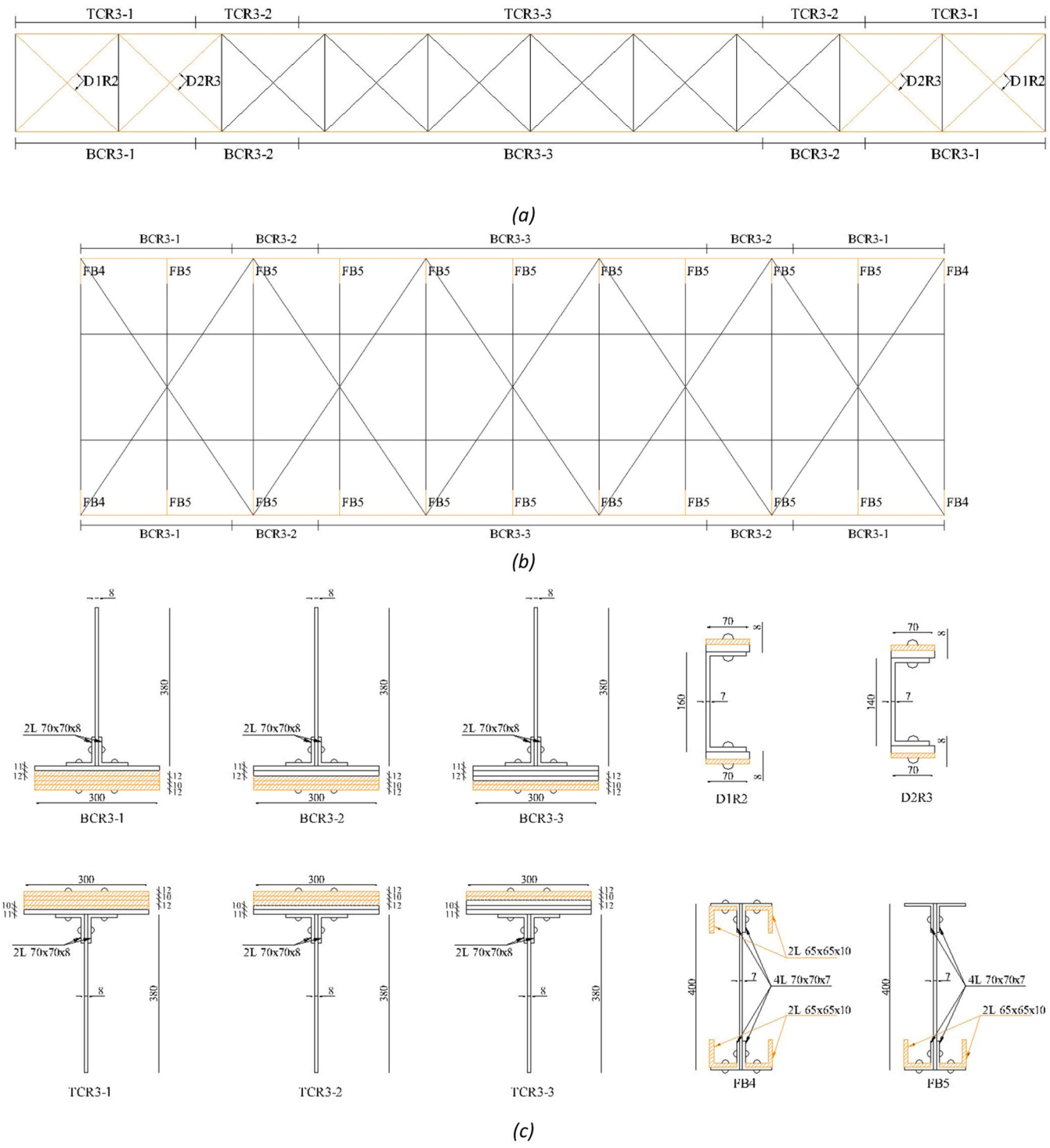

Fig. 12. Retrofitting of Bridge A members in 2021 (orange represents the retrofitting). Rivets of 20 mm with a separation of 60 mm are used for this retrofitting. Original drawing from EFE [96], redrawn by the authors (a): Bridge longitudinal view (b): Bridge transversal floor view (c): retrofitting of truss' bottom and top chords, truss' diagonals and floor beams.

freight, which are usually most commonly used for freight loads [42–64, 67,121].

The historic annual summaries from *EFE* [45–64], together with Nunez [65] and Marin [66,67], provide the mean annual freight load per wagon ($\overline{f_w}$). From 1914 to 1927, $\overline{f_w}$ can be determined as an approximate value function of the total freight load, the number of wagons per travel (n_w) and the annual locomotive frequency.

As can be seen from Fig. 17, where $\overline{f_w}$ is shown between 1907 and 1959, the average percentual load per wagon shows an increasing trend, except for 1921–1927. The percentage wagon's capacity ($C_{w\%}$) is determined using Eq. (5) by assuming an average of 30 tonnes of load capacity per wagon (C_w), and three linear trends are defined, as shown in Table 3, to have a better approximation of the data and determine $C_{w\%}$ for each year.

$$C_{w\%} = \frac{\overline{f_w}}{C_w} \tag{5}$$

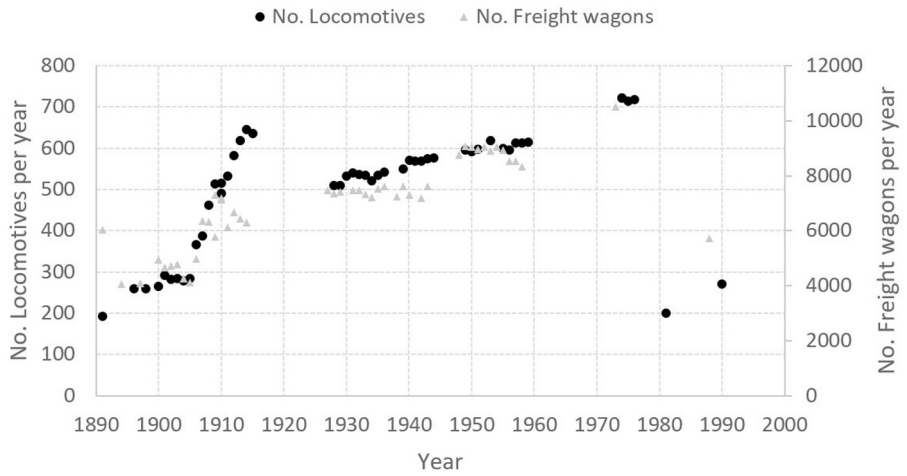

Fig. 13. No. of Locomotives and freight wagons used in the Chilean railway line in 1890–2000. Recreated from data taken from EFE annual summaries [42–64], Marin [66,67], León [68] and Simms [123].

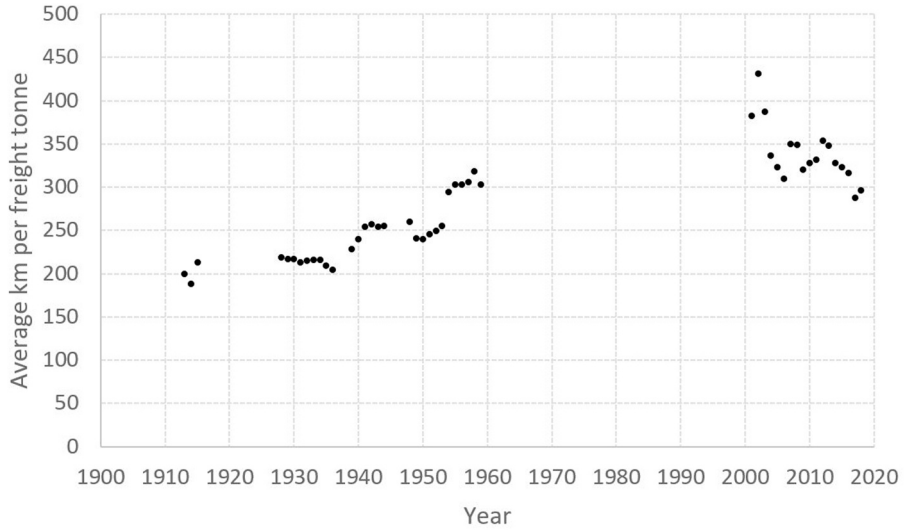

Fig. 14. Average km travel per one freight tonne in the Chilean railway line. Data compiled from ton-km given in EFE and Fepasa annual summaries.

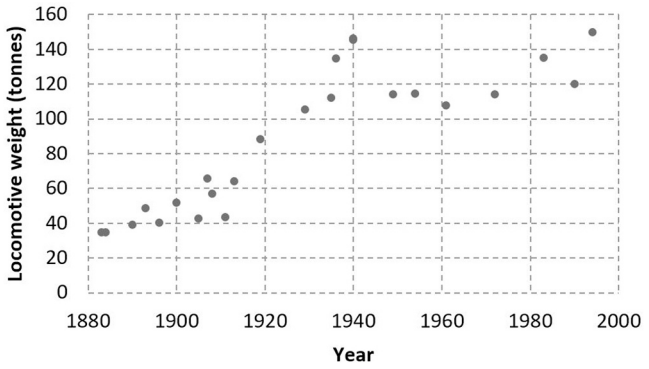

Fig. 15. Total axle's weight of locomotives used in Chile (not including the tender's weight for steam locomotives).

The percentage freight load per wagon is approximately 56% of the maximum wagon's capacity in the1900s, 67% in the 1910 s, 71% in the 1920 s, 66% in the 1930 s, 73% in the 1940 s, and 86% in the 1950 s, reaching a maximum of 95% of the load capacity in 1958 and 1959. This information is used to determine the axle load of each wagon (w_L) by

Table 2
Number and locomotives types owned and used by Fepasa company in the 5'6'' gauge in 2004, 2012 and 2021.

Type	2004	2012	2021
	No.	No.	No.
LDR-2300	23	23	23
LDR-1800	12	12	11
LER-3200	6	5	4
LDR-3300	-	3	9

following the Matlab routine shown in Fig. 18, using the average value of $C_{w\%}$ used for that period, considering the linear trends shown in Fig. 17. For the four periods between 1971 and 2022, $\overline{f_w}$ is assumed to be equal to C_w, as the trend shown in Fig. 17 display a tendency to reach the wagon maximum capacity.

The authors believe that the number of wagons increased with the introduction of diesel locomotives compared to the number of wagons used with the steam locomotives. However, this information could not be confirmed and, therefore, was not included in the analysis of the number of wagons per year.

Given the location and conditions of the bridge, the maximum C_w is

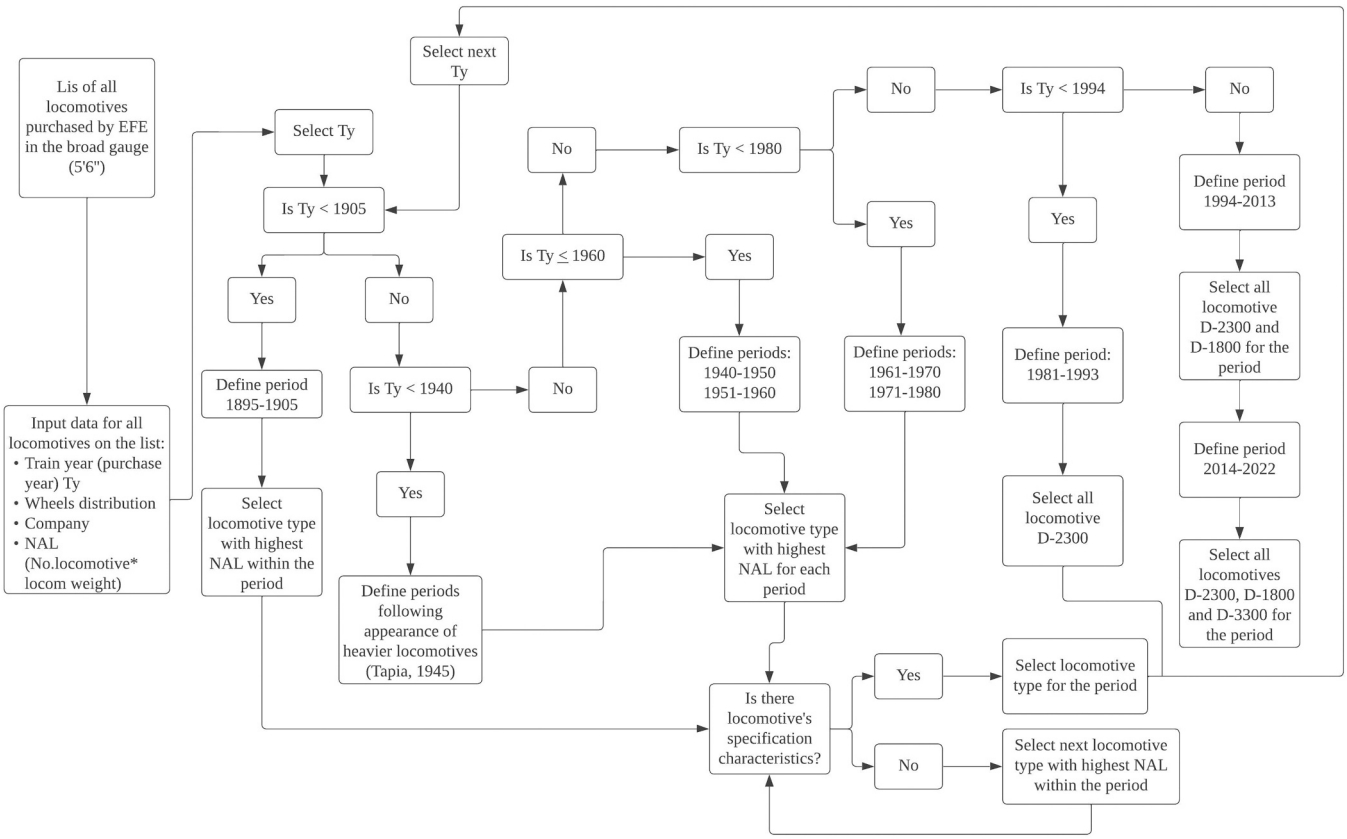

Fig. 16. Process to determine periods of the loading spectra and their representative locomotives.

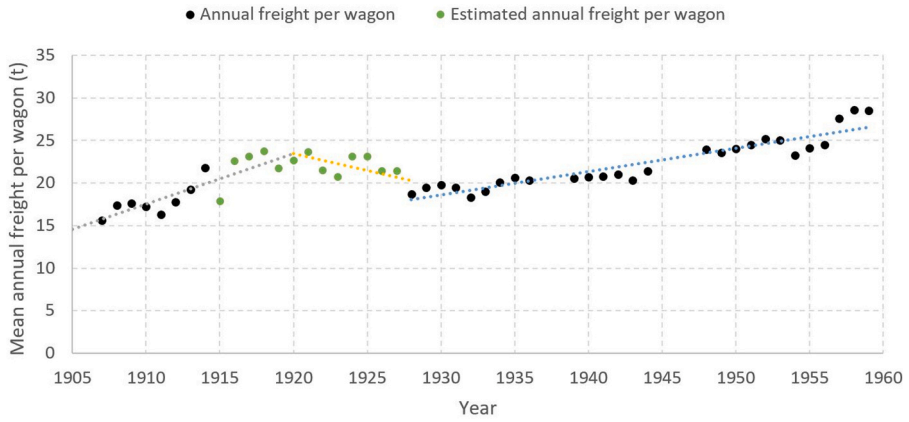

Fig. 17. Mean annual load per wagon used for freight transportation in the South of Chile (data taken from [45–67]).

Table 3
Mean annual percentage wagon capacity $C_{W\%}$.

	Annual percentage of wagon capacity
From 1895 to 1920	$C_{w\%} = 0.0198 \bullet year - 37.171$
From 1921 to 1927	$C_{w\%} = -0.0134 \bullet year + 26.423$
From 1928 to 1980	$C_{w\%} = 0.0094 \bullet year - 17.44$

restricted to 30 tonnes per wagon, although the wagons specified for the period between 1994 and 2022 for the locomotives D-1800 and D-3300 could carry up to 50 tonnes each.

The parameter n_w for each period is established following an exponential trend of the data presented in the annual summaries of EFE from 1930 to 1944 [45–56]. For the periods containing years within 1929 and 1950, n_w is determined as the integer round up of the average n_w in the period. For those periods comprised between 1895 and 1928, and 1951 to 2013, n_w for each year is determined using Eq. (6), and the integer round-up of the average n_w within the period is taken. For the last period (2014–2022), 35 wagons per each train are assumed, following recommendations from *EFE* and direct observation during the fieldwork carried out in 2021 by the authors.

$$n_w = 3 \bullet 10^{-9} \bullet e^{0.0115 \bullet year} \tag{6}$$

As all wagons are four-axle cars, w_L is then calculated following Eq. (7), where the tare load of each wagon and the freight load per wagon are considered.

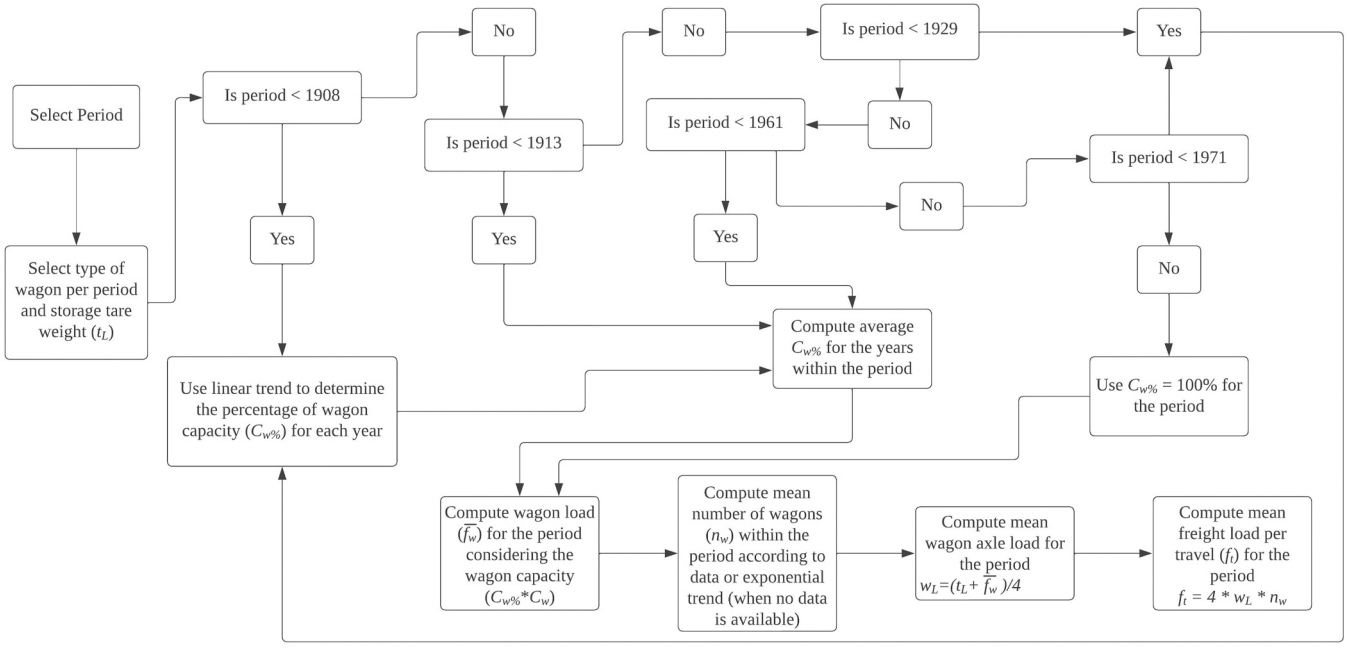

Fig. 18. Process to determine wagon freight load, number of wagons and wagon axle load for each period.

$$w_L = \frac{\overline{f_w} + t_L}{4}(tonnes) \quad (7)$$

With w_L it is then possible to determine the freight load per travel (f_t) by using Eq. (8), which will later be used to determine the annual train frequency for each period.

$$f_t = 4 \bullet w_L \bullet n_w(\mathrm{t/travel}) \quad (8)$$

5.3. Trains occurrence and composition

The train occurrence for each period is determined considering the

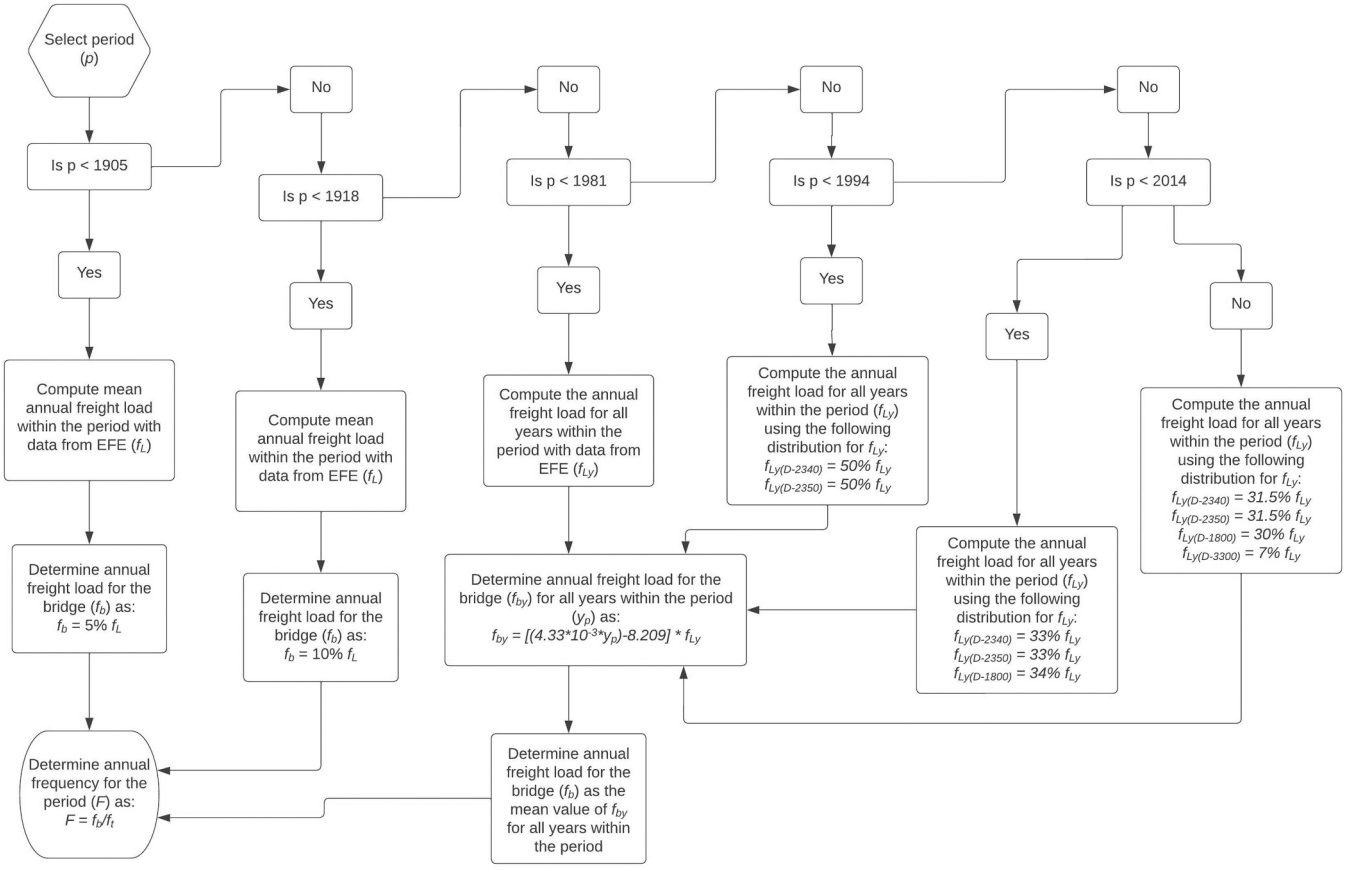

Fig. 19. Process to define the annual freight load over the year, the mean load for the periods, and the annual trains frequency for the loading spectra.

freight load per year summarised in Fig. 6. Until 1955, most freight was transported within the *south network*. identified in the annual summaries of *EFE* as the network between Valparaiso and the south of Puerto Montt, comprising more than 1100 km [43,64]. Bridge A is located close to the southern end of the network and therefore the proportion of all freight transiting over it needs to be considered. Only two relevant data points are available: in 1929, the freight load travelling was approximately 15% of the annual total freight load [44], and in 2019, this value had increased to 54% [83]. Considering a linear interpolation between these two values, the annual freight assumed to transit over the bridge (f_{by}) can be computed as a percentage of the total annual freight load ($\%f_{Ly}$) in each year (y), as per Eq. (9):

$$f_{by} = \%f_{Ly} = \left(4.33 \bullet 10^{-3} \bullet y\right) - 8.209(\mathrm{t/year}) \tag{9}$$

For periods with more than one representative locomotive, f_{Ly} is distributed according to the number of locomotives shown in Table 2 to determine the freight percentual load of each train, as shown in Fig. 19.

Before 1918 the mean annual freight load for the period (f_b) is assumed constant at 10% of the mean annual freight load (f_L) for the periods 1905–1907, 1908–1912 and 1913–1918 and 5% f_L for the period from 1895 to 1904, as shown in Fig. 19. For the rest of the periods, f_b is determined as an average of the freight loads of the years within the period (f_{by}). For each period, the train annual frequency (F) is determined considering the mean annual freight load for the period (f_b) over the freight load per travel (f_t):

$$F = \frac{f_b}{f_t}\left(\frac{travels}{yr}\right) \tag{10}$$

A summary of the details of the loading spectra obtained with this process for the fatigue analysis, is shown in Table 4, including the locomotive manufacturer and model, length of the locomotive with tender, the ratio between the length of the locomotive plus tender and the length of the bridge (L_{L+T}/L_B), the ratio between the length of the wagon and the length of the bridge (L_W/L_B), wagon axle loads, the ratio between the tare load and the freight load of each wagon ($t_L/\overline{f_w}$), number of wagons per train and number of annual journeys estimated, to be of relevance to bridge A given the total annual freight load. From this information an annual journey histogram for each train combination and period in service is shown in Fig. 20.

As previously stated, the locomotives chosen to represent each period were selected according to their weight and number of units. As the heavier locomotives are usually selected, the fatigue damage results presented in this study should be conservative compared to actual traffic data, where all locomotive models that transit over the bridge are considered. The annual traffic should also give a conservative approximation of the actual number of transits, therefore, the assumptions made for this investigation could tend to overestimate the fatigue damage of the bridge.

6. Numerical models

The bridge is modelled using the commercial software SAP2000 v19.2.1 [126]. Four 3D numerical models are generated to assess the fatigue damage of the bridge caused by the train loads defined in Section 5, and following all bridge configurations; initial (Fig. 21), 1927 retrofitting (Fig. 22), 1935 retrofitting (Fig. 23) and 2021 retrofitting (Fig. 24). All models have two pinned supports at one end of the bridge, that restrict all displacement but allowing rotation, and two rollers at the other end to allow longitudinal movement and free rotation. The number of elements and nodes of each model is summarised in Table 5.

All models use four-node shell elements for stringers, floor beams, truss chords, verticals and end-posts, with equivalent cross-sections with the same depth (d) and second moment of area as the built-up members. Only the diagonals of the truss girders and floor diagonals are modelled through frame elements with hinged connections at both ends to ensure that they work as truss elements. A refined mesh is considered in proximity of the connection, as seen in the close-up of Fig. 21(a) and Fig. 22 where the red dots show the location on the stringer where the stress histories are analysed. Fig. 21(b) and Fig. 24(b) also displays the application of the axle loads as point loads over to top flange of the stringers.

Table 4
Type of trains and traffic details for different periods impacting Bridge A.

Time Period	Locomotive Type	Length of locomotive and tender (m)	L_{L+T}/L_B Ratio	L_W/L_B Ratio	Wagon Axle Load (t)	$t_L/\overline{f_w}$ Ratio	No. Wagons	Freight Load (t/year)	Annual Frequency
1895-1904	Rogers (4-6-0)	13.67	0.89	0.69	6.3	0.9	9	107960	476
1905-1907	A. Borsing (0-6-0)	11.04	0.72	0.69	7.9	0.9	10	307306	979
1908-1912	North British (4-6-0)	13.74	0.90	0.69	8.8	1.0	11	414465	1067
1913-1918	Baldwin (4-6-0)	13.74	0.90	0.69	10.1	0.8	11	482195	1086
1919-1926	Mikado (4-8-2)	18.12	1.18	0.72	8.8	0.7	12	618532	1458
1929-1934	Mountain (4-8-2)	20.05	1.31	0.72	8.7	0.7	13	1001604	2217
1940-1950	Baldwin (4-8-2) (Type 80 EFE)	20.05	1.31	0.79	9.5	0.8	14	1531881	2879
1951-1960	Alco-GE RSC2	12.57	0.82	0.79	10.5	0.8	18	1976036	2614
1961-1970	D-1600	13.42	0.88	0.79	11.4	0.7	20	2141542	2343
1971-1980	D-1800	15.53	1.02	0.83	11.7	0.6	22	2108538	2048
1981-1993	D-2340	12.68	0.83	0.83	11.7	0.5	25	916976	784
	D-2350	12.68	0.83	0.83	11.7	0.6	25	916976	784
1994-2013	LDR-2340	12.68	0.83	0.83	11.7	0.6	30	1285302	915
	LDR-1800	15.53	1.02	0.84	11.9	0.6	30	1324251	929
	LDR-2350	12.68	0.83	0.83	11.7	0.6	30	1285302	915
2014-2022	LDR-2340	12.68	0.83	0.84	11.9	0.6	35	1777410	1069
	LDR-2350	12.68	0.83	0.84	11.9	0.6	35	1777410	1069
	LDR-1800	15.53	1.02	0.83	11.7	0.6	35	1692771	1033
	LDR-3300	16.98	1.11	0.84	11.9	0.6	35	394980	238

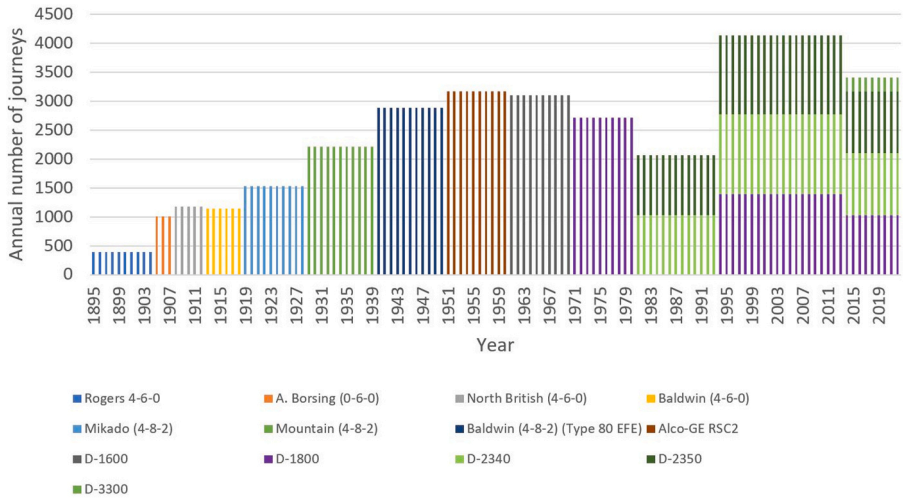

Fig. 20. Representative locomotives and their annual frequency for Bridge A.

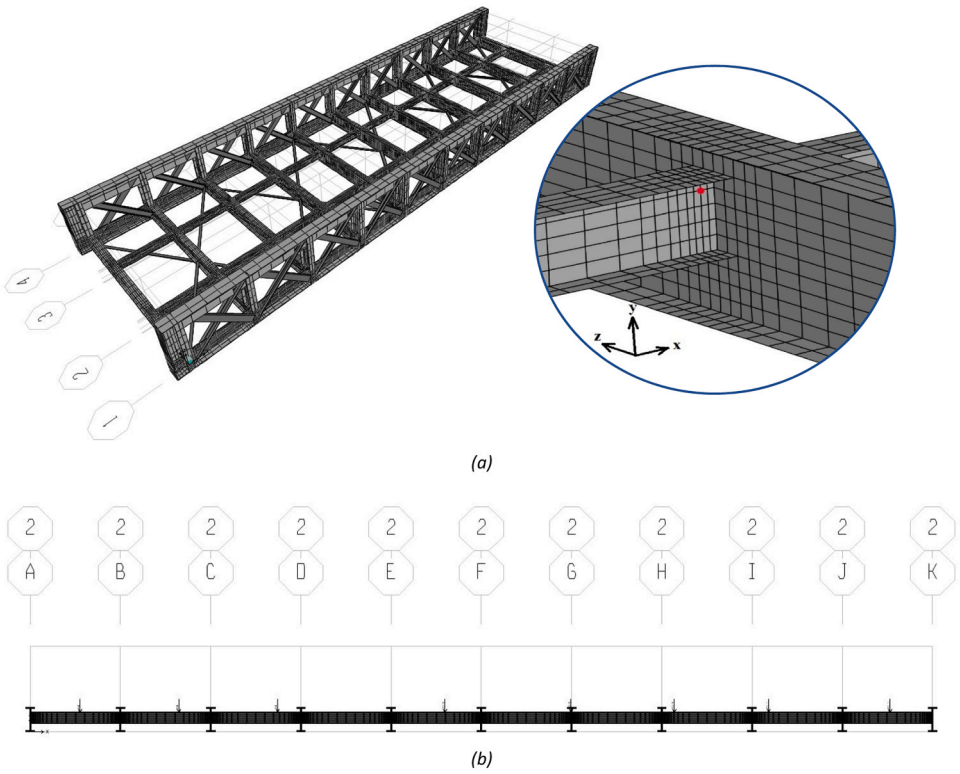

Fig. 21. (a) 3-D model of Bridge A without retrofitting (model INI) with close-up details of stringer-to-floor-beam connections. (b) 2D View of one set of stringers with Baldwin train axle loads, step 30.

Although most fatigue assessments with global models are made through frame elements [10,11,17], the use of shells elements in the truss girder and floor system allows for a better representation of the relative stiffness between these members, as well as 2D state of stress allows to consider explicitly principal stresses and shear stresses, and it is therefore chosen for the numerical FE models.

The stringer-to-floor-beam and floor-beam-to-lower-chord riveted connections are modelled as fully fixed by tying these members together at the connection's location. The full continuity increases the bending stress near the connection while reducing the midspan bending stresses [127] and it is a common assumption for riveted connections and fatigue damage in heritage bridges [10,15,28].

An elastic static analysis is performed considering a Young Modulus of 210 GPa, Poisson ratio of 0.36 and steel density of 78.5 kN/m^3 according to the specifications given by *EFE* [91]. As previously described, the yield and ultimate strength are assumed to be 240 and 360 MPa, respectively.

The train loads are applied directly to the top flange of stringers in progressing steps of 0.5 m. to simulate the moving train, while the dead load due to sleepers and rails is applied as an additional uniform load to the stringers. The load spread due to sleepers and rails, and the interaction between axle and rails, are neglected.

7. Fatigue analysis and results

The following assumptions are made for the fatigue analysis of

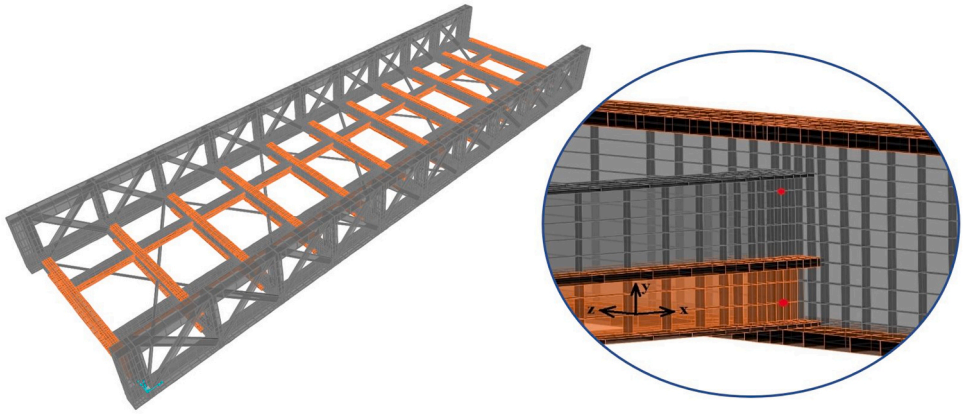

Fig. 22. 3-D model of Bridge A with 1927's retrofitting (model R1) and close-up details of stringer-to-floor-beam connections. Orange colour represent the retrofitting.

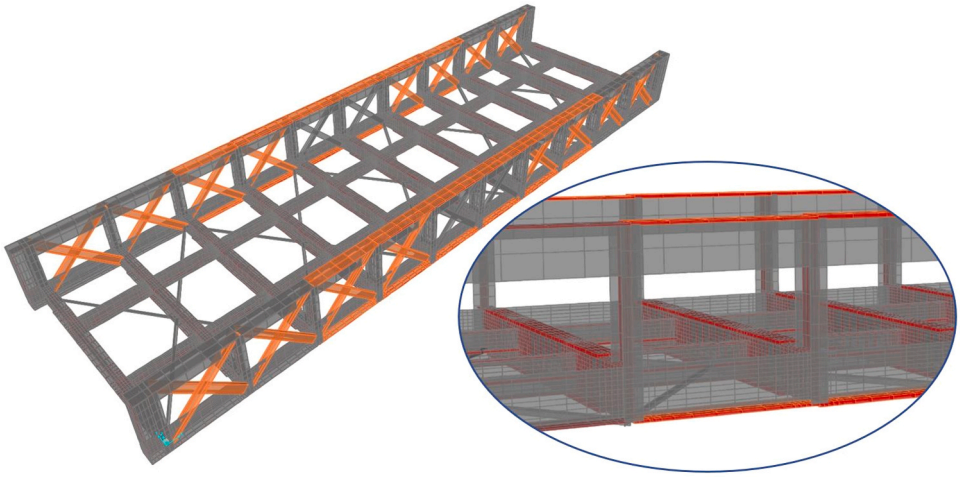

Fig. 23. 3-D model of Bridge A with 1935's retrofitting (model R2) and close-up details of added plates in top and bottom chords. Orange colour represent the retrofitting.

Bridge A:

- The bridge in its initial configuration was considered to be unaltered until 1927.
- The only interventions on the bridge are the ones described in the retrofitting of 1927, 1935 and 2021.
- Any structural effect on the bridge associated with moderate or heavy earthquakes that occurred between 1895 and 2022 in Chile is not considered
- Fatigue S-N from EC3 are suitable since the bridge was built and designed by a French Company
- No replacement of structural members occurred during the strengthening interventions. However, they were carefully maintained to prevent corrosion. This assumption is critical when considering that the S-N curves have an endurance limit where small stress cycles do not contribute to fatigue, as when corrosion is acknowledged the shape of the S-N curves differs and the infinite fatigue strength vanishes [128]. Therefore, in this study it is assumed that the fatigue damage is a cumulative phenomenon on the members' connection, given that the changes in the structural configuration of the bridge's members affected only the stress distribution on the elements resulting from the train passing.
- No degradation of mechanical properties was considered for the bridge's members that were not replaced in any of the retrofitting events.

The bridge connections that are assessed are identified as $S_i{-}FB_j/FB_{j+1}$, where S and FB are stringers and floor beams, respectively, and i and j indicate the position of members according to the nomenclature shown in Fig. 25. The train traffic is assumed to be transiting in equal proportion from North to South and South to North (50%−50%).

The stress results on the stringer-to-floor beam connection shows that the connection is affected by bending and shear stress. Fig. 26 shows that the stress variation between σ_1 and σ_x is less than 30% for most of the response, however in some train positions the shear stress τ_{max} is significant and σ_1 is 60 to 70% higher than σ_x.

For Bridge A in its initial configuration (Model INI), the flexural stiffness of the stringer is lower than the connecting floor beam, producing a hogging moment near the stringer-to-floor-beam connection, generating tension in the top of the connection. However, once the bridge is retrofitted (Models R1 and R2), the relative stiffness between the stringers and floor beam switches, and then the bottom of the stringer is in tension. This becomes less noticeable by the third retrofitting (Model R3) when the floor beam is further retrofitted. This effect is illustrated in Fig. 27, where σ_x without amplification factors applied is displayed for both the top and bottom of the stringer-to-floor-beam connection.

For the case of the bridge in its initial configuration, fatigue damage extends to all stringers-to-floor-beams connections, as it is caused by both locomotive and wagon transit. The Baldwin train is the one that

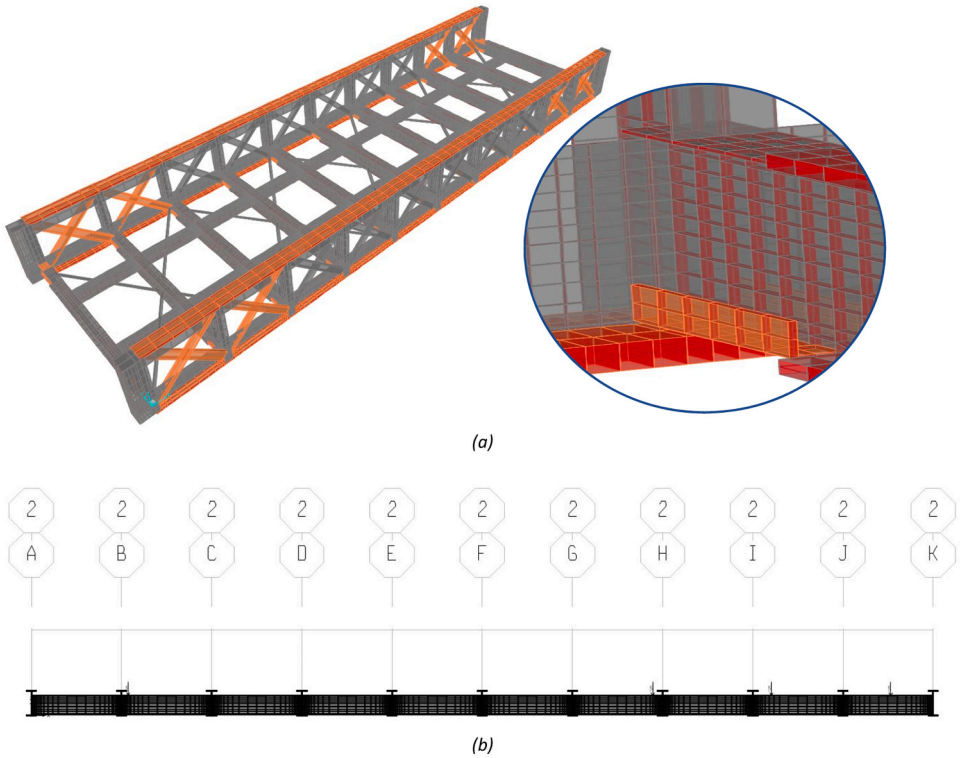

Fig. 24. (a) 3-D model of Bridge A with 2021's retrofitting (model R3) and close-up details of floor-beam-to-bottom-chord connection at mid-span. Orange colour represent the retrofitting (b) 2D View of one set of stringers with the D-3300 train axle loads applied as point loads in train step 30.

Table 5
Number of elements and nodes for each bridge model.

Model	Initial Configuration (INI)	1927 Retrofitting (R1)	1935 Retrofitting (R2)	2021 Retrofitting (R3)
Frame Elements	60	60	60	60
Surface Elements	27214	31782	32166	32934
Nodes	28633	33511	33965	34871

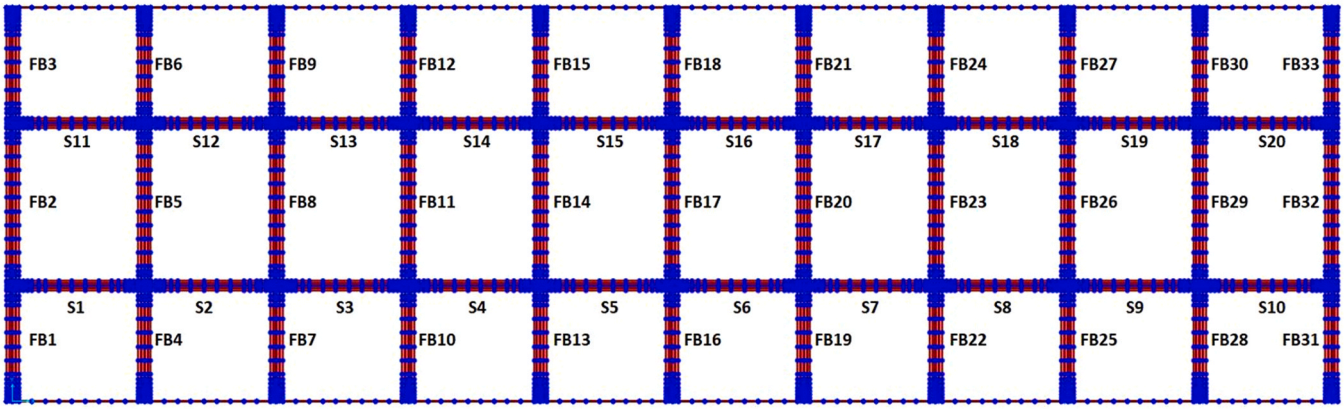

Fig. 25. Nomenclature of stringers and floor beams position in the bridge floor system.

produces greater fatigue damage, as it trails 11 wagons with 101 KN axle load, while the Mikado train, although heavier than the Baldwin, trails 88 KN axle load wagons and therefore produces lower accumulate fatigue damage (see Fig. 28, where the stress response and rainflow counting with EC3 category detail 63 is shown in the most damaging stringer-to-floor-beam connection for each train, with the train progresses from left to right). As the axle loads of the locomotive are greater in magnitude and at closer distance, the maximum stress is produced in the left end side stringer-to-floor-beam connections, while, given the short span of the bridge compared to the length of the train, the following cycles reflect the contributions of only wagons, with axle loads further spaced away and with smaller magnitude, causing lower maximum stress to the right end of the bridge.

The results for the fatigue damage D due to a single train transiting from stringer S1 to S10, computed by using Eq. (4) with $t_j = y_j = 1$, are presented in Fig. 29 for the four configurations of the structure and

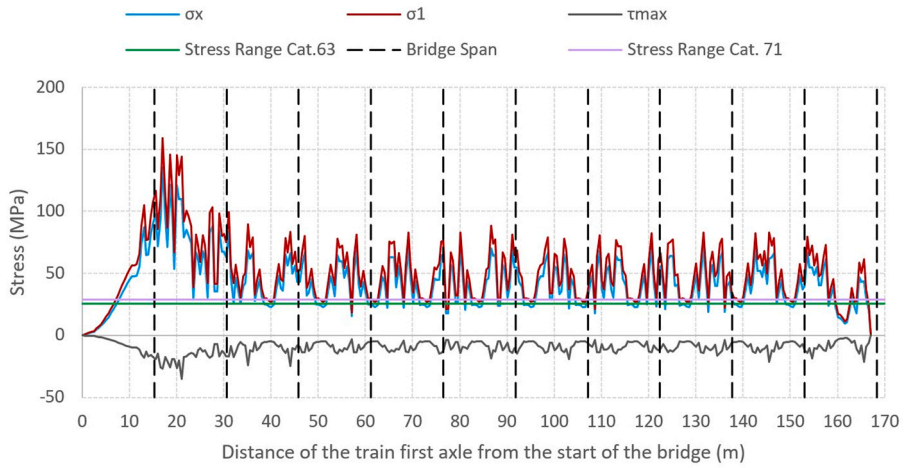

Fig. 26. Amplified stress response in stringer-to-floor-beam connection due to passage of train Mikado with 12 wagons for the bridge in its initial configuration.

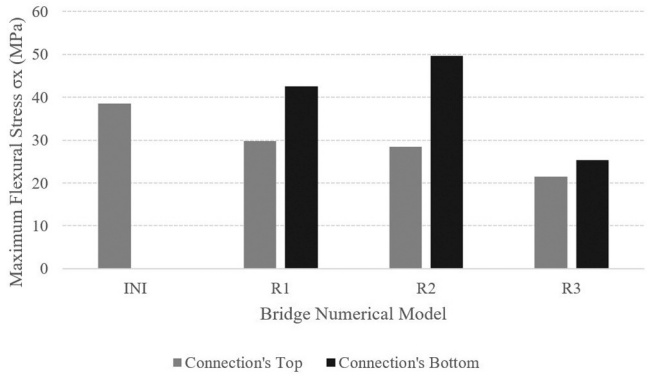

Fig. 27. Non-amplificated σ_x (MPa) for each numerical model at the top and bottom of the stringer-to-floor-beam connection under the maximum stress step.

corresponding train models for each period, respectively, for each of the stringers' connections. The fatigue damage *D* is expressed as the proportion of total number of fatigue cycle causing damage, as indicated by the S-N curves [34]. The results shown in Fig. 29 corresponds to the Category 63 S-N curve, which are higher than the results with Category 71. As the bridge is symmetric, the damage of one set of stringers (S1 to S10) is equal to the other set (S11 to S20).

For the bridge in its initial configuration and with the final retrofitting, the fatigue damage determined with the S-N curve category detail 71 is approximately 35% lower than with 63 category detail, because of the greater *Se* of the former. On the other hand, the fatigue damage determined for the other bridge configurations (R1 and R2) with category detail 63 is approximately one order of magnitude greater than the damage obtained with category detail 71. Moreover, the fatigue damage obtained with the heaviest train for the bridge in its initial configuration is approximately 90% greater than the damage determined with the heaviest train during the retrofitting periods of R1 and R2 for both category details.

With each retrofitting, the bridge increased its stiffness and strength, and the stress response on the connection was reduced when comparing the bridge response with the same train for different retrofitting configurations, as shown in Fig. 30. In this case, the fatigue damage index, *DI*, with the retrofitting is more than six times smaller than the fatigue damage with the bridge in its initial configuration (INI), due to a reduction on the number of stress ranges that contribute to fatigue. However, as every retrofitting was implemented, the trains also evolved, as shown in the loading spectra. Therefore, although the bridge was stiffer, it was also subjected to heavier loads. As seen in Fig. 31, where the stress response is compared for each bridge configuration with the

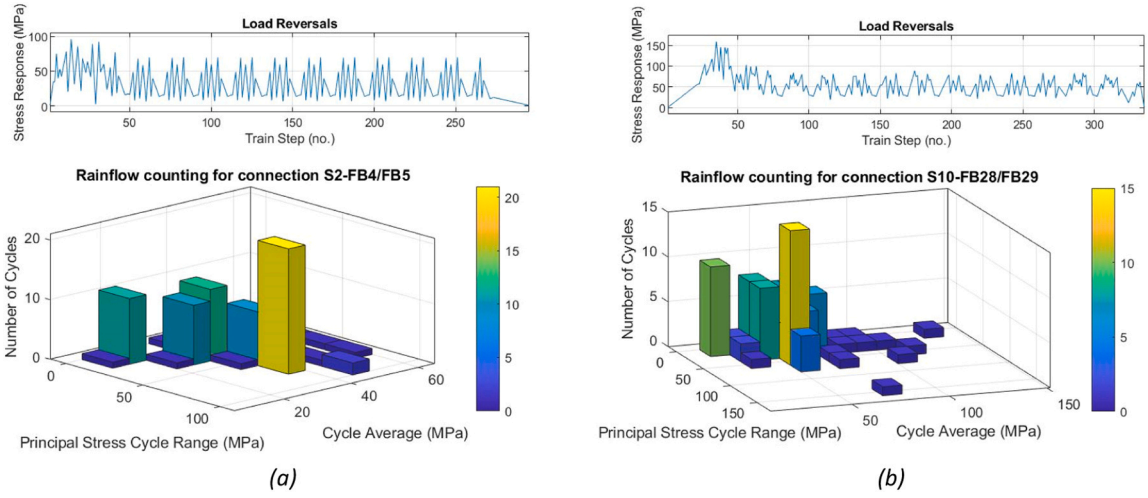

Fig. 28. Rainflow counting and 3D stress histogram for one stringer-to-floor-beam connection of the bridge in initial configuration. (a) Response with train Baldwin with 11 wagons (b) Response with train Mikado with 12 wagons.

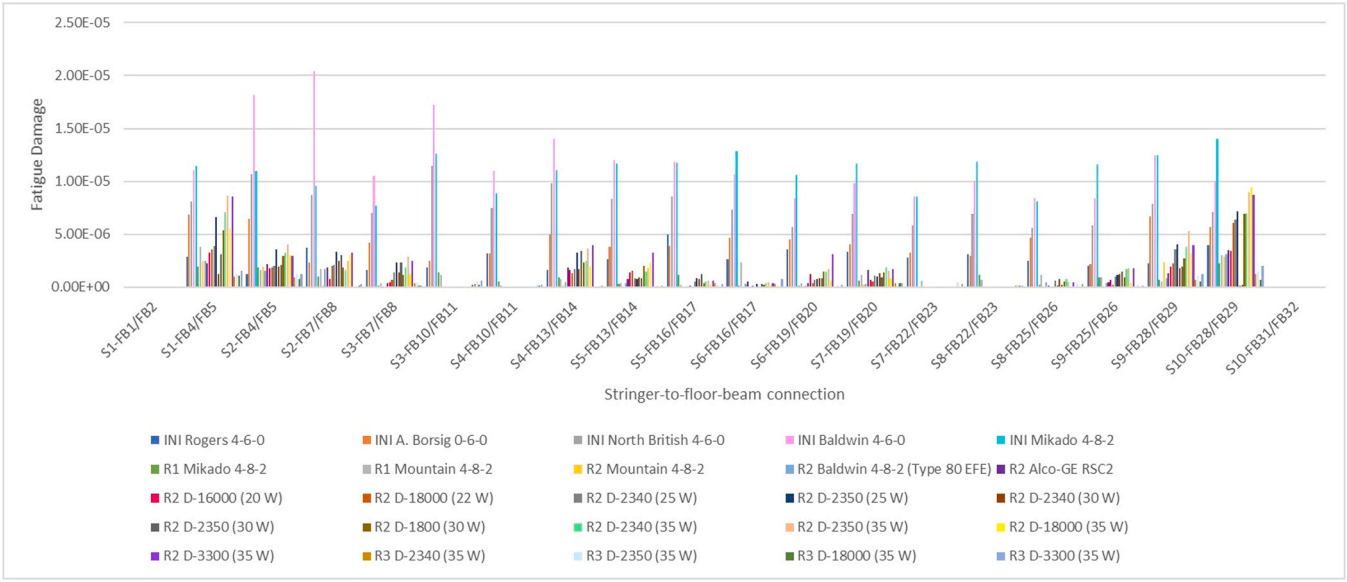

Fig. 29. Fatigue damage in stringer-to-floor-beam connection for as-built bridge (INI), with 1927 retrofitting (R1), with 1935 retrofitting (R2) and 2021 retrofitting (R3) due to a single train passage in the period from 1895 to 1926 (INI), 1927 to 1934 (R1), 1935 to 1973 (R2) and 2021 to 2022 (R3) with S-N Curve Category Detail 63.

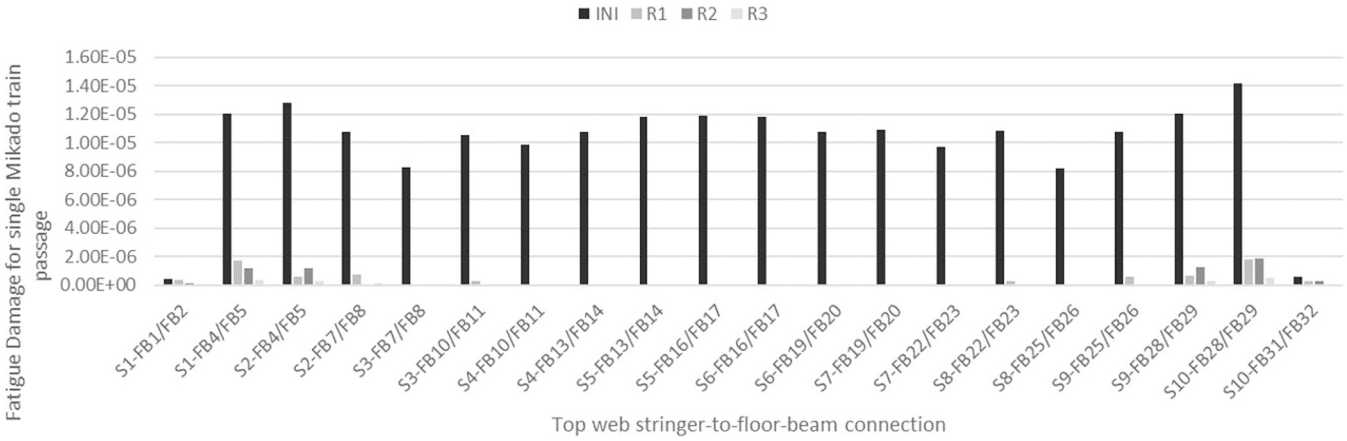

Fig. 30. Fatigue damage comparison with different Bridge A configurations (INI, R1, R2 and R3) with passage of train Mikado 4–8-2 with 12 wagons and S-N Curve category detail 63.

heavier train during the retrofitting period (locomotive plus wagons weight), greater damage was produced on the bridge in its initial configuration. Nonetheless, comparable damage is obtained for connections S1-FB4/FB5 and S10-FB28/FB29 with the heaviest train of the period in the INI and R2 bridge configuration, respectively (see Fig. 31a).

The accumulated fatigue damage index (*DI*) determined through Eq. (4) with the amplified principal stress and the yearly occurrence established in the loading spectra is shown in Fig. 32 for both the top and bottom stringer-to-floor-beam connection. The value of *DI* greater than 1.0 in some connections indicates that the amplification factor used for the stress response is highly conservative. This is further discussed the next section.

The initial configuration of the bridge produced similar fatigue damage *D* in all stringer-to-floor-beam connections. However, once the bridge was retrofitted, the first set of stringers were the ones subjected to greater number of fatigue cycles (see Fig. 29). The new configurations consistently caused a shift of the most fatigue-vulnerable location from top to bottom for the stringers located close to 1/3 of the bridge span, as shown in Fig. 32.

The average fatigue damage per year produced in each stringer-to-floor-beam connection with every bridge retrofitting, including the initial configuration, is shown for both the top in Fig. 33(a), and bottom of the connection, Fig. 33(b). This damage was determined considering the value of DI for the period of each configuration divided by the number of years within that period. As shown in Fig. 33(a), the fatigue damage at the top of the connection is mainly produced by the bridge configurations INI and (R2), as heavier trains are in use during this last period. This shows that although the retrofitting of the bridge allows for the use of heavier trains, the fatigue produced was still significant on the stringer-to-floor-beam connections in the first panels of the bridge. Similarly, greater damage at the bottom of the connection at one-third of the bridge span, is obtained with configuration R2, as shown in Fig. 33 (b). This is due to greater bending effects in the fourth panel, generating stress cycles with greater amplitude and mean value, as shown in Fig. 34. The maximum stresses are located in steps 15 and 41 for the passage of the heavier train D-3300, and on those train steps, the maximum σx in the connections are located between the third and fourth bridge panel, as shown in Fig. 35. The position of the train in these two steps are also shown in Fig. 35, and they look similar because

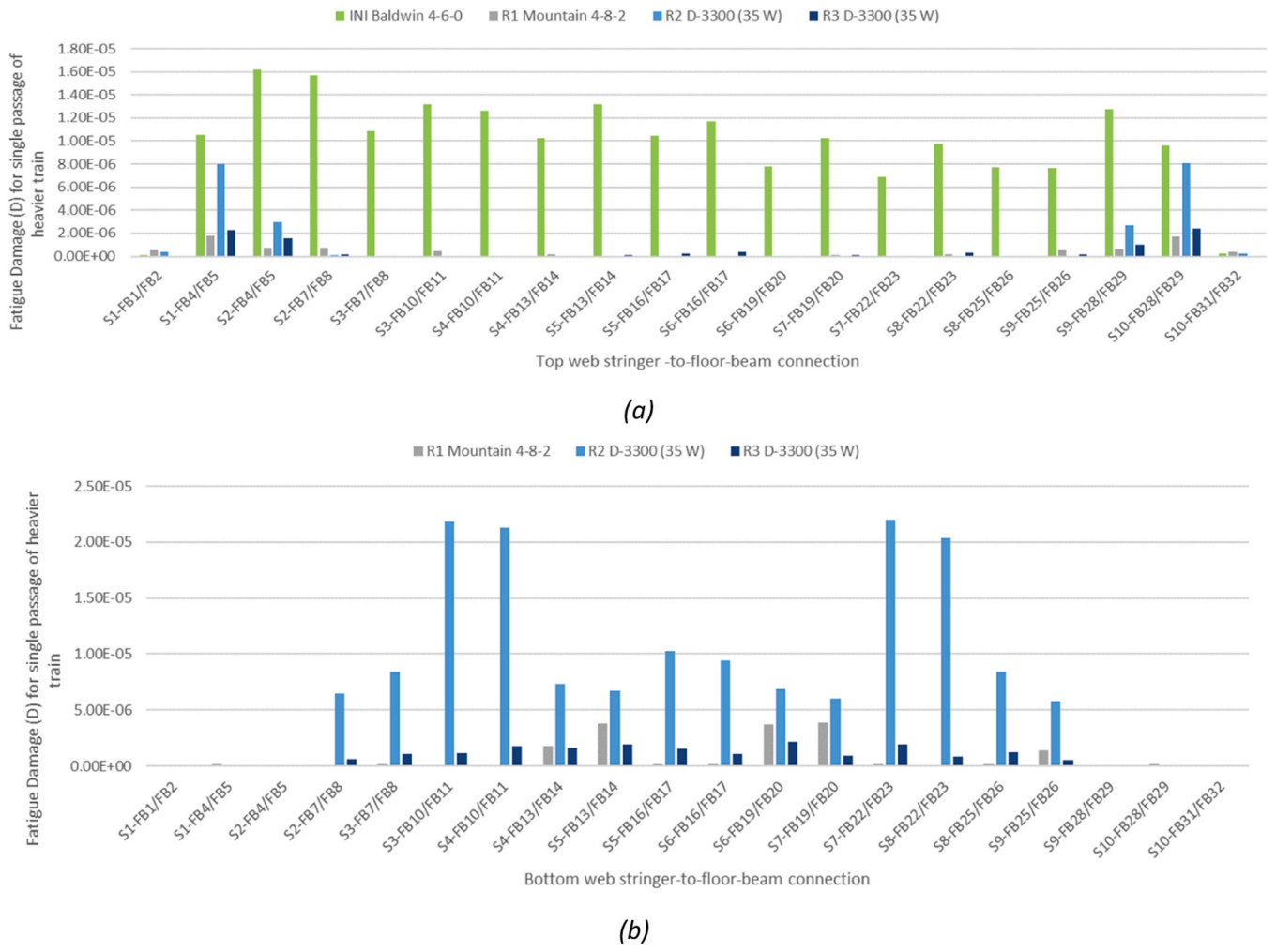

Fig. 31. Fatigue damage for different Bridge A configurations (R1, R2 and R3) with passage of the heaviest train during the corresponding period and S-N Curve category detail 63 (a) On the top of the stringer-to-floor-beam connection (b) On the bottom of the stringer-to-floor-beam connection.

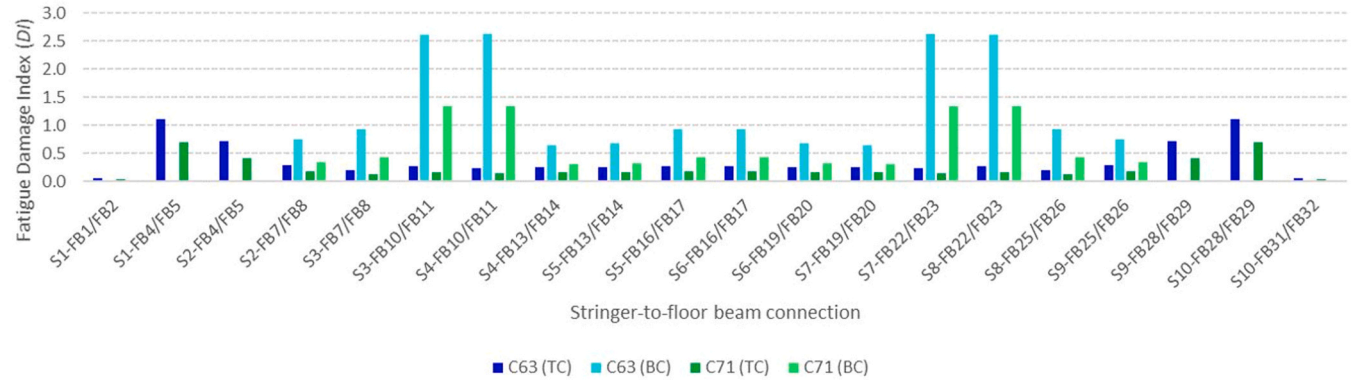

Fig. 32. Fatigue damage Index, DI, representing the accumulated fatigue damage for the top (TC) and bottom (BC) of the stringer-to-floor-beam connection with S-N Curve Category Detail 63 and 71.

the locomotor D-3300 has 6 axles in total, and the separation between the first three axles with the following three axles is almost 9 m. It is important to notice that the flexural stress distribution shown in Fig. 35 is not amplified because it is shown over the length of the bridge and not only at the connection's positions, where the Af used considers the SCF in the riveted connections. Therefore, should be noted that the stress shown in the connections of Fig. 35 should be amplified to obtain the stress response shown in Fig. 34.

The fatigue damage is also assessed with the bridge in its current configuration, with all interventions but without considering the sequence and timing of interventions. The whole life loading spectrum (see Table 4) is applied to configuration R3. Then the fatigue damage index *DI* is determined by applying Eq. (4). In this case, the total fatigue damage is significantly underestimated, as the most damaged upper stringer-to-floor-beam connection results are reduced by approximately 75%, as shown in Fig. 36. For the bottom stringer-to-floor-beam

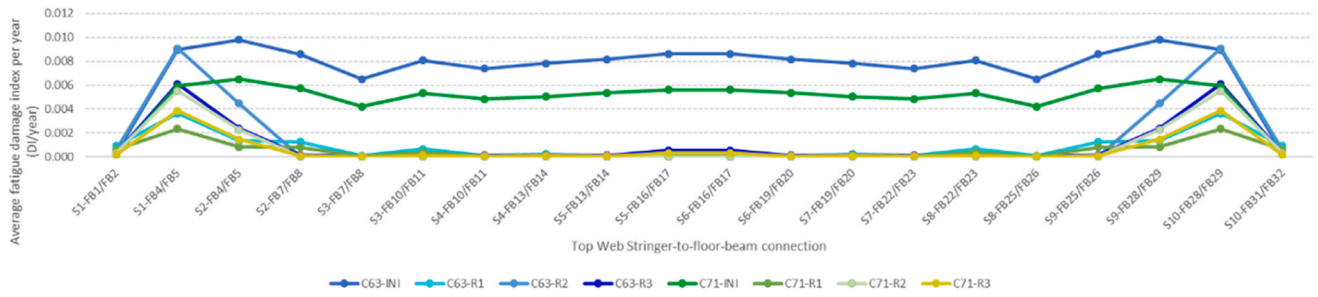

(a)

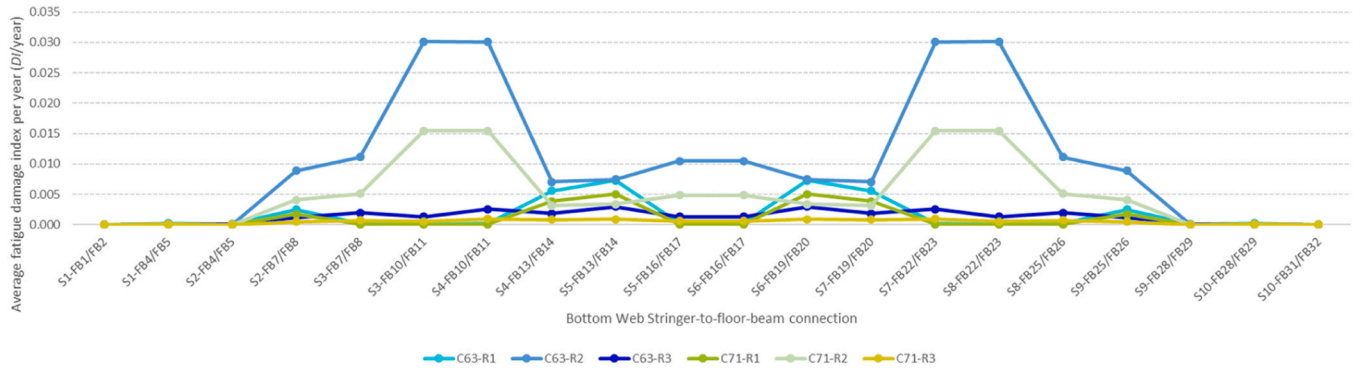

(b)

Fig. 33. Average fatigue damage per year in stringer-to-floor-beam connections with the bridge in different configurations (INI, R1, R2 and R3). Results are shown for Category Detail 63 (C63) and 71 (C71). (a) Top of the stringer-to-floor-beam connection. (b) Bottom of the stringer-to-floor-beam connection.

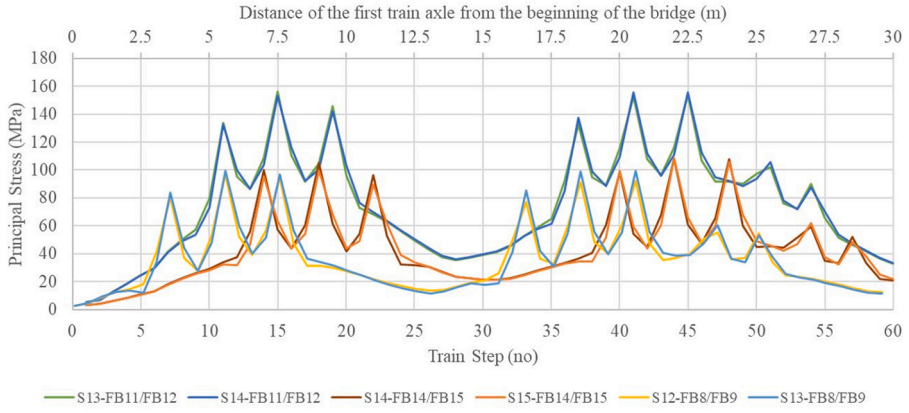

Fig. 34. Principal tensile stress response σ_1 in different R2 bridge stringer-to-floor-beam connections due to passage of locomotor D-3300.

connection, the results are even more underrated, completely overlooking the damage associated with configuration R2. Therefore, the history of retrofitting is as critical to a realistic fatigue damage assessment as the loading sequence.

8. Sensitivity analysis

As previously shown, the results are susceptible to the stress response, which depends on the loads applied and the amplification factor used for analysis, besides other factors such as the configuration, the connection-fixity and the use of principal vs flexural stresses.

In this section, the use of a lower amplification factor and the use of flexural stresses are presented to show the differences in the fatigue damage calculation.

Although σ_1 is higher than σ_x, the percentual difference between these maximum values is low. However, for a train step were the stress is at a minimum point, σ_x could be significantly lower than σ_1, leading to a greater stress range. This case is displayed in Fig. 37 for the passage of the first 50 m of train D-2350 with 20 wagons (corresponding to the locomotor plus two wagons) over the bridge configuration R2. For the maximum stress points, (black boxes), σ_1 is greater than σ_x by 5 to 10%, while for the minimum values (green boxes) σ_x is up to 100% smaller than σ_1. Therefore, as the stress range with σ_x is greater than with σ_1, the fatigue damage is more significant because of the reduced number of cycles associated with higher stress ranges. Thus, the accumulated fatigue damage for the bridge increases.

The use of different amplifications factors (A_f) also influences the overall fatigue damage, as can be seen in Fig. 38, where the accumulated fatigue damage is shown for both the top and bottom of the connection with a lower amplification factor of 1.9, which corresponds to the *SCF*

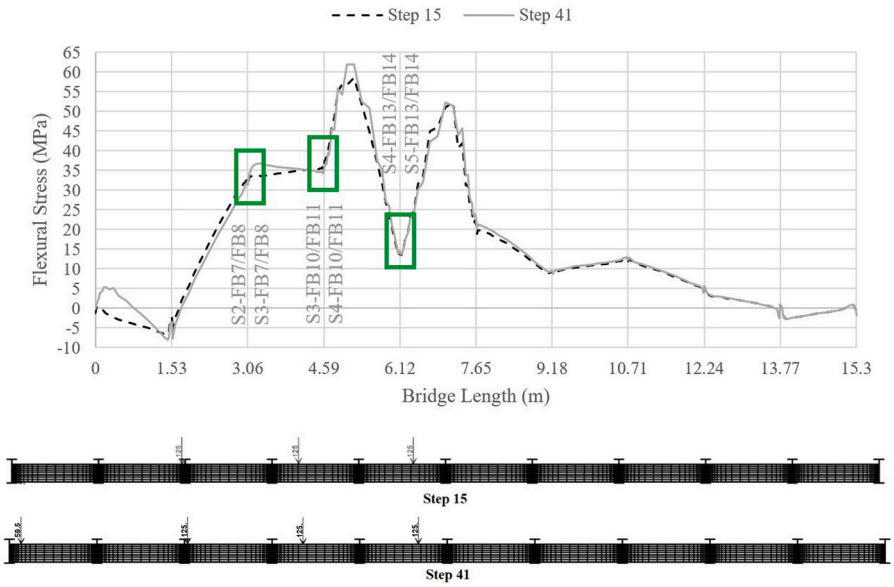

Fig. 35. Flexural stress σ_x over the R2 bridge with the locomotor D-3300 in the step 15 and step 41.

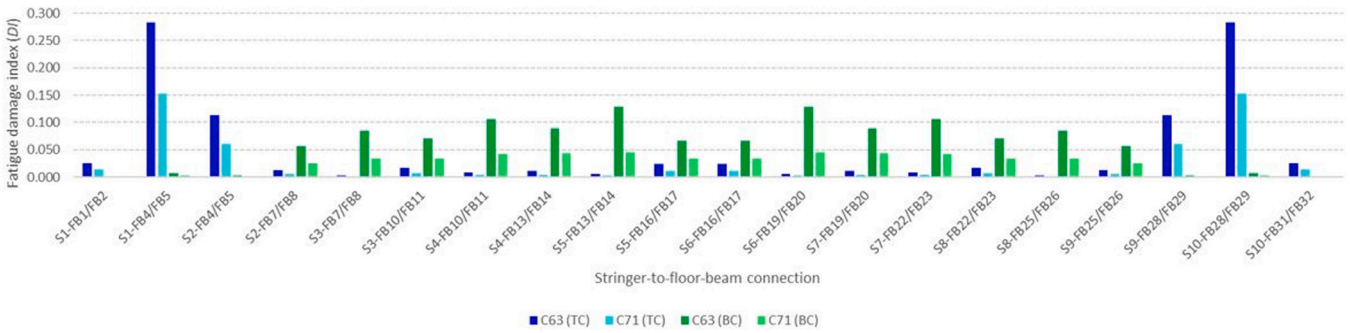

Fig. 36. Accumulate fatigue damage for the bridge in its current configuration for the top (TC) and bottom (BC) of the stringer-to-floor-beam connection with S-N Curve Category Detail 63 and 71.

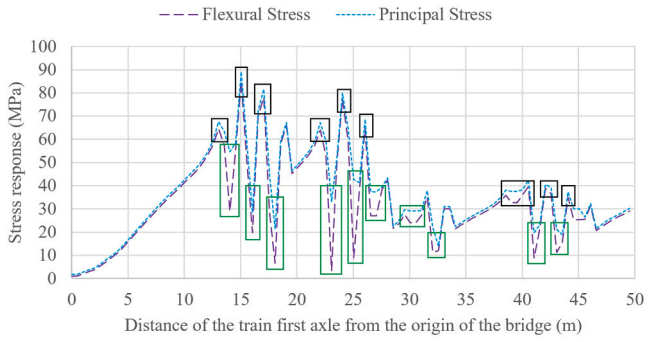

Fig. 37. Flexural (σ_x) and principal (σ_1) stress response on the stringer-to-floor-beam connection S9-FB28/FB29 of bridge R2 within the first 50 m of Train D-2350 with 20 wagons.

obtained from the relation by Marques [17], in comparison with the amplification factor used for the fatigue analysis and shown in the methodology.

Fig. 38 shows that *DI* is not proportional to the amplification factor. Although the stress response and, therefore, the stress range is proportional to the decreasing amplification factor used, the number of cycles associated with that range increases more significantly by following Eq. (3) and as shown in Fig. 39. For example, with $\sigma_a = 76\ MPa$ (A_f =2.9), N_i is 3.5 times lower than with $\sigma_a = 50\ MPa$ (A_f =1.9).

Similarly, the use of different amplification response factors when using σ_x greatly influences the fatigue damage, as shown in Fig. 40.

Although the results regarding fatigue damage are sensitive to the considerations used to estimate the response, the results presented in this section show that the connection identified as more prone to fatigue damage is the same in all cases.

9. Conclusions

Thanks to the available drawings and documentation of all interventions made to a Chilean riveted Howe bridge, this study presents a novel assessment of fatigue damage that considers principal tensile stresses, a detailed and realistic loading spectrum based on real data of trains and frequency, and all structural configuration changes to the bridge during its 127 years of life. This study shows that to assess fatigue all of this information is essential. It is also evident that several assumptions are necessary when information is incomplete or qualitative, as it will be the case for most historic bridges. A proper record and account of the uncertainties that ensue is essential to the reliability of the outcome and how this influence the decision on the future of the bridge.

The fatigue damage was determined using S-N Curves Category Detail 63 and 71 of the EC3. The total fatigue damage index *DI*, calculated by applying Miner's rule, shows that the results are sensitive to the category detail's selection, as the index is reduced by approximately 35

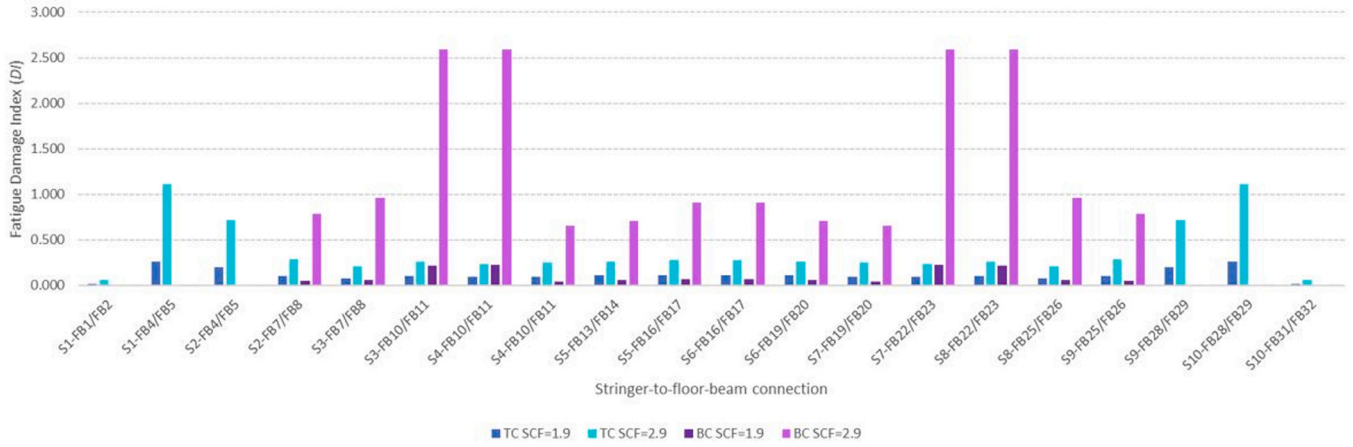

Fig. 38. Fatigue damage index with different amplification factors in the stringer-to-floor-beam connection's top and bottom, considering σ_1 response.

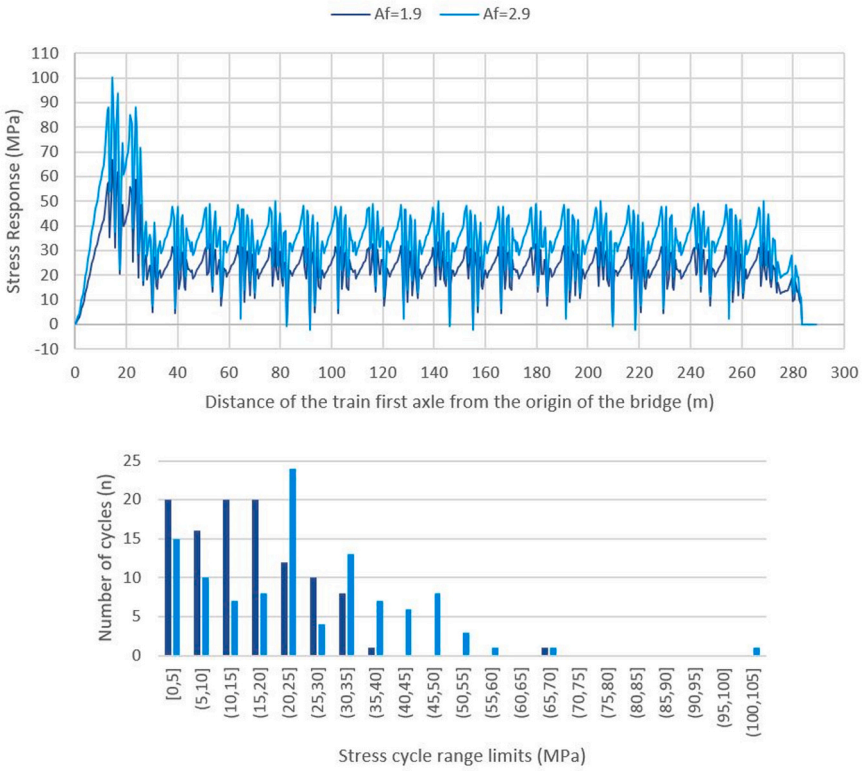

Fig. 39. Principal stress response and stress range histogram of connection S9-FB28/FB29 with train D-2350 and 20 wagons with different amplification factors.

to 50% at the stringer-to-floor-beam connections of the bridge when determining fatigue damage by using category detail 71 in comparison with category detail 63.

As the fatigue damage index *DI* obtained with this analysis is greater than 1, considering both category detail 63 and 71, it can be concluded that the amplification factor used for the stress response in the connection (A_f) overestimate the fatigue damage, and a more suitable factor should be determined, considering the implication for the corresponding number of relevant cycles. The use of flexural versus principal stress values is also critical to the determination of the damage index. Loading assumptions on the periods where data was scarce might be overestimated, impacting the overall results of *DI*.

From the fatigue analysis, it can be concluded that configuration R3 of the bridge is sufficient to endure fatigue cycles, as the stress ranges produced from the passage of trains are substantially lower than the ones produced by configuration R2, even considering a high amplification factor.

The position of the most fatigue-prone connections is linked to the change in bridge configuration, which affects the stress distribution in the connections by changing the floor member's stiffness. For this case study, stringer-to-floor-beams connections identified as S14-FB11/FB12 and S17-FB23/FB24 are more prone to fatigue damage when considering the historic sequence of configuration and train loading. These elements experienced more fatigue-damaging cycles when the tensile stresses were located in the bottom flange of the stringer-to-floor-beam connection, which occurs for configurations R1 and R2.

Although the bridge could experience more significant damage by a given train model, the fatigue damage index also depends on the train frequency. Therefore, the loading spectra to perform the fatigue analysis must represent the accurate loading over the bridge. The loading model

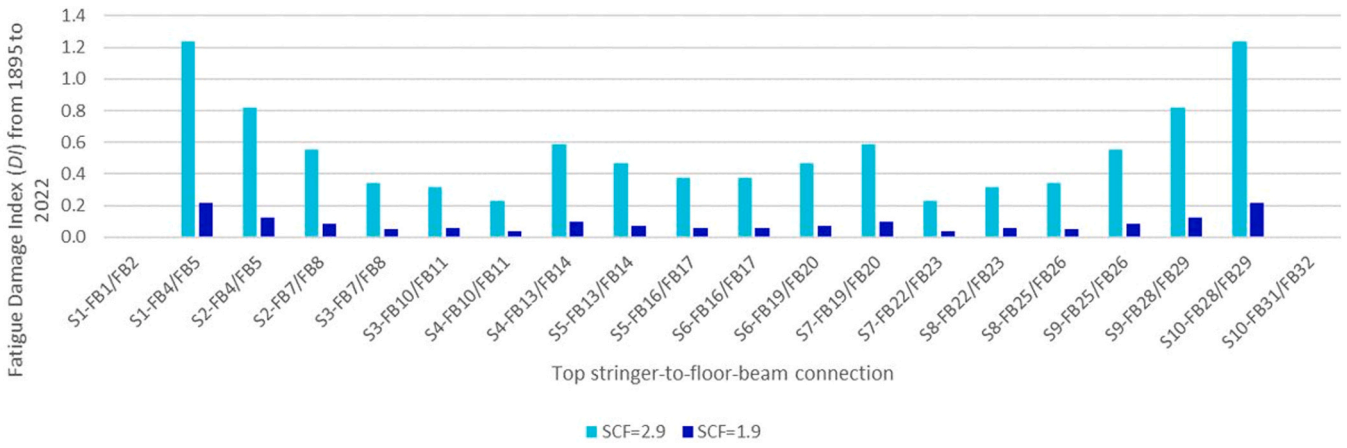

Fig. 40. Comparison of fatigue damage index considering σ_x with different amplifications factors at the top of the connection.

developed for this study considers the frequency of different trains over time and representative freight loading with different wagon tare loads. Moreover, it includes a detailed analysis of the freight tonnage that transited over the bridge since its construction date, giving an accurate estimate of the bridge's live load throughout its life. The authors are working on a second publication to compare the fatigue damage to different railway bridge's classes in Chile considering a detailed load spectrum vs the fatigue damage given using load models suggested by different Standards and Codes.

Although the structure is stiffer and stronger with R2 than with R1, the bridge fatigue damage is higher for R2. This is because of the heavier trains and the large number of passages, as the R2 configuration was in place for 86 years.

The fatigue damage assessment is significantly affected by analysing the bridge in its current configuration without considering the prior configurations. Therefore, knowing the history of the bridge and all interventions made to the structure is of great importance for adequately assessing the fatigue damage in the structure.

As the results are highly sensitive to the amplification factors used for the riveted connections, the authors plan to use local FE models to determine a more realistic stress response for the riveted connections.

CRediT authorship contribution statement

Camila Parodi-Figueroa: Conceptualization, Data curation, Formal analysis, Investigation, Methodology, Visualization, Writing – original draft, Writing – review & editing. **Dina D'Ayala:** Conceptualization, Formal analysis, Supervision, Validation, Writing – review & editing, Methodology. **Wendel Sebastian:** Formal analysis, Methodology, Supervision, Validation, Writing – review & editing.

Declaration of Competing Interest

The authors declare the following financial interests/personal relationships which may be considered as potential competing interests: Camila Parodi-Figueroa reports financial support was provided by Chilean National Agency for Research and Development. If there are other authors, they declare that they have no known competing financial interests or personal relationships that could have appeared to influence the work reported in this paper.

Data Availability

Data will be made available on request.

Acknowledgements

The authors wish to thank the Chilean National Agency for Research and Development ANID BECAS CHILE/DOCTORADO EN EL EXTRANJERO 72190308 for their financial support in this investigation.

References

[1] SB-LRA. Guideline for load and resistance assessment of existing european railway bridges – advises on the use of advance methods. Eur Res Proj Prep Sustain Bridges EU 2007:FP6.
[2] Olofsson I, Elfgren L, Bell B, Paulsson B, Niederleithinger E, J, S, Bien J. Assessment of European railway bridges for future traffic demands and longer lives – EC project "Sustainable Bridges". Struct Infrastruct Eng 2005;1(2):93–100.
[3] Imam BM, Chryssanthopoulos MK. Causes and consequences of metallic bridge failures. Struct Eng Int: *J Int Assoc Bridge Struct Eng (IABSE)* 2012;22(1):93–8.
[4] Kühn, B., Lukić, M., Nussbaumer, A., Günther, H., Helmerich, R., Herion, S.,. Bucak, O. (2008). Assessment of existing steel structures: Recommendations for estimation of remaining fatigue life. Joint Report. Prepared under the JRC-ECCS cooperation agreement for the evolution of Eurocode 3 (programme of CEN/TC 250). In: Sedlacek, G.; Bijlaard, F.; Géradin, M.; Pinto, A.; Dimova, S. editors. 1st ed.
[5] Imam, B. (2006). Fatigue Analysis of Riveted Railway Bridges. PhD Thesis. University of Surrey, UK.
[6] Pipinato A, Pellegrino C, Modena C. Fatigue assessment of highway steel bridges in presence of seismic loading. Eng Struct 2011;33:202–19.
[7] Rageh A, Azam SE, Linzell DG. Steel railway bridge fatigue damage detection using numerical models and machine learning: Mitigating influence of modeling uncertainty. Int J Fatigue 2020;134:105458.
[8] Haghani R, Al-Emrani M, Heshmati M. Fatigue-prone details in steel bridges. Buildings 2012;2(4):456–76.
[9] Heydarinouri H, Nussbaumer A, Motavalli M, Ghafoori E. Strengthening of steel connections in a 92-year-old railway bridge using prestressed cfrp rods: multiaxial fatigue design criterion. J Bridge Eng 2021;26(6). https://doi.org/10.1061/(ASCE)BE.1943-5592.0001714.
[10] Spyrakos C, Raftoyiannis I, Ermopoulos J. Condition assessment and retrofit of a historic steel-truss railway bridge. J Constr Steel Res 2004;60(8):1213–25.
[11] Ermopoulos J, Spyrakos C. Validated analysis and strengthening of a 19th century railway bridge. Eng Struct 2006;28(5):783–92.
[12] Liu Z, Correia J, Carvalho H, Mourão A, Jesus A, Calçada R, Berto F. Global-local fatigue assessment of an ancient riveted metallic bridge based on submodelling of the critical detail. Fatigue Fract Eng Mater Struct 2019;42(2):546–60.
[13] Franz H, Lepretre E, Chataigner S, Rinke M, Dieng L. Assessment of the rotational stiffness of single-riveted joints in a steel lattice girder by modal analysis. Eng Struct 2024;298:117052. https://doi.org/10.1016/j.engstruct.2023.117052.
[14] Marques, F. (2016). Fatigue Assessment of Old Riveted Railway Bridges. PhD Thesis. Universidade Do Porto, Portugal.
[15] Imam BM, Righiniotis TD, Chryssanthopoulos MK. Numerical modelling of riveted railway bridge connections for fatigue evaluation. Eng Struct 2007;29:2071–3081.
[16] Carter JW. Stress concentrations in built-up structural members. Proc Am Railw Eng Assoc 1952;53:1–34.
[17] Marques F, Correia JAFO, Jesus AMP, Cunha A, Caetano E, Fernandes AA. Fatigue analysis of a railway bridge based on fracture mechanics and local modelling of riveted connections. Eng Fail Anal 2018;94:121–44.
[18] Federal Emergency Management Agency, F.–5. (2006). Techniques for the Seismic Rehabilitation of Existing Buildings. Retrieved from http://www.fema.gov/.

[19] D'Ayala D. Conservation principles and performance based strengthening of heritage buildings in post-event reconstruction. Geotech. Geol Earthq Eng 2014; 34:489–514.
[20] Tapia, J. (1945). Refuerzo de Puentes Metálicos de los FF. CC. Del E (Chile). Talleres Gráficos de los Ferrocarriles del Estado.
[21] Frøseth G, Rönnquist A. Load model of historic traffic for fatigue life estimation of Norwegian railway bridges. Eng Struct 2019;200:109626.
[22] Shao YH, Chen L, Xu Y, Cao S. Widening and Strengthening of the Songpu Bridge. *Struct Eng Int: J Int Assoc Bridge Struct Eng* (IABSE) 2019;29(3):354–61.
[23] Roberts C, Hanson A, Henderson D, Bell G. Jamestown Viaduct, UK: strengthening of an early steel viaduct. Proc Inst Civ Eng Bridge Eng 2007;160(2): 57–63.
[24] Wallin J, Leander J, Karoumi R. Strengthening of a steel railway bridge and its impact on the dynamic response to passing trains. Eng Struct 2011;33(2):635–46.
[25] Bell, B. (n.d.). Strengthening metallic bridges Network Rail's experiences. Network Rail Presentation.
[26] Kaibler, F.W., Dunker, K.F., Wipf, T.J., & Sanders, W.W. (1987). Methods of strengthening existing highway bridges. National Cooperative Highway Research Program Report 293. Washington, D.C.: Transportation Research Board. National Research Council.
[27] Kim JB, Brungraber RJ, Yadlosky JM. Truss bridge rehabilitation using steel arches. J Struct Eng (N Y, N Y) 1984;110(7):1589–97.
[28] Brencich A, Gambarotta L. Assessment procedure and rehabilitation of riveted railway girders: the Campasso Bridge. Eng Struct 2009;31(1):224–39.
[29] Kossakowski PG. Fatigue strength of an over one hundred year old railway bridge. Balt J Road Bridge Eng 2013;8(3):166–73. https://doi.org/10.3846/bjrbe.2013.21.
[30] Imam B, Salter PA. Historical load effects on fatigue of metallic railway bridges. Bridge Eng 2017;171(1):49–62.
[31] Akesson, B. (1994) Fatigue Life of Riveted Railway Bridges. PhD thesis, Chalmers University of Technology, Gothenburg, Sweden.
[32] UIC (International Union of Railways) (1986) UIC Code 779–1 R: Recommendations for determining the load carrying capacity of existing metal structures. UIC, Paris, France.
[33] Al-Emrani. Fatigue performance of stringer-to-floor-beam connections in riveted railway bridges. J Bridge Eng 2005;10(2):179–85. https://doi.org/10.1061/(ASCE)1084-0702(2005)10:2(179).
[34] EN 1993–1-9 (2005) Eurocode 3: Design of steel structures – Part 1–9: Fatigue.
[35] Cremona C, Eichler B, Johansson B, Larsson T. Improved assessment methods for static and fatigue resistance of old metallic railway bridges. J Bridge Eng 2013;18 (11):1164–73.
[36] Pipinato A. Step level procedure for remaining fatigue life evaluation of one railway bridge. Balt J Road Bridge Eng 2010;5(1):28–37.
[37] Miner MA. Cumulative damage in fatigue. J Appl Mech 1945;12(3):A159–64.
[38] Chandran KSR, Chang P, Cashman GT. Competing failure modes and complex S–N curves in fatigue of structural materials. Int J Fatigue 2010;32(3):482–91. https://doi.org/10.1016/j.ijfatigue.2009.08.004.
[39] Wilson, W.M. and Thomas, F.P. (1938). Fatigue test of riveted joints. In Engineering Experiment Station.University of Illianois: Urbana.
[40] EFE. (2002). Norma Técnica Ferroviaria. Diseño de Puentes Ferroviarios. EFE-NTF-13–001. Empresa de Ferrocarriles del Estado.
[41] MATLAB and Statistics Toolbox Release R2019b, The MathWorks, Inc., Natick, Massachusetts, United States
[42] Ferrocarriles del Estado de Chile (1892). Octava memoria presentada al señor Ministro de Industria y Obras Publicas por el Director Jeneral de los Ferrocarriles del Estado 1891. Santiago de Chile, Imprenta Cervantes.
[43] Ferrocarriles del Estado de Chile (1911). Vijesimo septima memoria presentada por el Director Jeneral de los Ferrocarriles del Estado al señor Ministro de Industria y Obras Publicas Correspondiente al año 1910. Santiago de Chile, Imprenta de los Ferrocarriles del Estado.
[44] Ferrocarriles del Estado (1930). 46a Memoria correspondiente al año 1929. Republica de Chile, Imprenta Nascimiento.
[45] Ferrocarriles del Estado (1931). 47a Memoria correspondiente al año 1930. Santiago de Chile, Sociedad Imprenta y Litografia Universo.
[46] Ferrocarriles del Estado (1932). 48a Memoria correspondiente al año 1931. Santiago de Chile, Imprenta de Los Ferrocarriles del Estado.
[47] Ferrocarriles del Estado (1933). 49a Memoria correspondiente al año 1932. Santiago de Chile, Imprenta de Los Ferrocarriles del Estado.
[48] Ferrocarriles del Estado (1934). 50a Memoria correspondiente al año 1933. Santiago de Chile, Imprenta de Los Ferrocarriles del Estado.
[49] Ferrocarriles del Estado (1935). 51a Memoria correspondiente al año 1934. Santiago de Chile, Imprenta de Los Ferrocarriles del Estado.
[50] Ferrocarriles del Estado (1936). 52a Memoria correspondiente al año 1935. Santiago de Chile, Imprenta de Los Ferrocarriles del Estado.
[51] Ferrocarriles del Estado (1937). 53a Memoria correspondiente al año 1936. Santiago de Chile, Talleres Gráficos de los Ferrocarriles del Estado.
[52] Ferrocarriles del Estado (1941). 57a Memoria correspondiente al año 1940. Santiago de Chile, Talleres Gráficos de los Ferrocarriles del Estado.
[53] Ferrocarriles del Estado (1942). 58a Memoria correspondiente al año 1941. Santiago de Chile, Talleres Gráficos de los Ferrocarriles del Estado.
[54] Ferrocarriles del Estado (1944). 59a Memoria correspondiente al año 1942. Santiago de Chile, Talleres Gráficos de los Ferrocarriles del Estado.
[55] Ferrocarriles del Estado (1944). 60a Memoria correspondiente al año 1943. Santiago de Chile, Talleres Gráficos de los Ferrocarriles del Estado.
[56] Ferrocarriles del Estado (1945). 61a Memoria correspondiente al año 1944. Santiago de Chile, Talleres Gráficos de los Ferrocarriles del Estado.
[57] Ferrocarriles del Estado (1951). 66a Memoria correspondiente al año 1949. Santiago de Chile, Talleres Gráficos de los Ferrocarriles del Estado.
[58] Ferrocarriles del Estado (1951). 67a Memoria correspondiente al año 1950. Santiago de Chile, Talleres Gráficos de los Ferrocarriles del Estado.
[59] Ferrocarriles del Estado (1952). 68a Memoria correspondiente al año 1951. Santiago de Chile, Talleres Gráficos de los Ferrocarriles del Estado.
[60] Ferrocarriles del Estado (1954). 70a Memoria - Año 1953.Santiago de Chile, Talleres Gráficos de los Ferrocarriles del Estado.
[61] Ferrocarriles del Estado (1954). Datos de los Servicios de la Empresa año 1953. Santiago de Chile, Talleres Gráficos de los Ferrocarriles del Estado.
[62] Ferrocarriles del Estado (1955). 71a Memoria - Año 1954. Santiago de Chile, Talleres Gráficos de los Ferrocarriles del Estado.
[63] Ferrocarriles del Estado (1961). 75a Memoria - Año 1958. Santiago de Chile, Talleres Gráficos de los Ferrocarriles del Estado.
[64] Ferrocarriles del Estado de Chile (1962). 76a Memoria - Año 1959. Santiago de Chile.
[65] Nunez, S. (1910) Los Ferrocarriles del Estado. Reseña Historica, Explotación y Diccionario Biográfico. Santiago de Chile, Imprenta I Encuadernacion Chile.
[66] Marin, S. (1901) Estudios de los Ferrocarriles Chilenos. Santiago de Chile, Imprenta Cervantes, Edición Publicada en los "Anales de la Universidad"
[67] Marin, S. (1916) Los Ferrocarriles de Chile. Santiago de Chile, Imprenta Cervantes, IV Edición.
[68] León, V. (2017). La decadencia del ferrocarril en la red centro sur de Chile (1950–1990). XVI Jornadas Interescuelas/Departamentos de Historia. Departamento de Historia. Facultad Humanidades. Universidad Nacional de Mar del Plata, Mar del Plata.
[69] Cabrera, F. (2016) Desarrollo Ferroviario en Chile: revisión de algunos antecedentes históricos y económicos. Biblioteca del Congreso Nacional de Chile/BCN. Departamento de Estudios, Extensión y Publicaciones, SSP3328.
[70] EFE (2010a) Memoria Anual 2003. Santiago de Chile. Available at ⟨https://www.efe.cl/corporativo/documentos/memorias-anuales/efe-trenes-de-chile/⟩.
[71] EFE (2010b) Memoria Anual 2004. Santiago de Chile. Available at ⟨https://www.efe.cl/corporativo/documentos/memorias-anuales/efe-trenes-de-chile/⟩.
[72] EFE (2010c) Memoria Anual 2005. Santiago de Chile. Available at ⟨https://www.efe.cl/corporativo/documentos/memorias-anuales/efe-trenes-de-chile/⟩.
[73] EFE (2010d) Memoria Anual 2006. Santiago de Chile. Available at ⟨https://www.efe.cl/corporativo/documentos/memorias-anuales/efe-trenes-de-chile/⟩.
[74] EFE (2010e) Memoria Anual 2007. Santiago de Chile. Available at ⟨https://www.efe.cl/corporativo/documentos/memorias-anuales/efe-trenes-de-chile/⟩.
[75] EFE (2010f) Memoria Anual 2008. Santiago de Chile. Available at ⟨https://www.efe.cl/corporativo/documentos/memorias-anuales/efe-trenes-de-chile/⟩.
[76] EFE (2010g) Memoria Anual 2009. Santiago de Chile. Available at ⟨https://www.efe.cl/corporativo/documentos/memorias-anuales/efe-trenes-de-chile/⟩.
[77] EFE (2010h) Empresa de Los Ferrocarriles del Estado Memoria Anual 2010. Santiago de Chile. Available at ⟨https://www.efe.cl/corporativo/documentos/memorias-anuales/efe-trenes-de-chile/⟩.
[78] EFE (2011) Memoria Anual 2011 Empresa de Los Ferrocarriles del Estado. Santiago de Chile. Available at ⟨https://www.efe.cl/corporativo/documentos/memorias-anuales/efe-trenes-de-chile/⟩.
[79] EFE (2012) Memoria Anual 2012 Empresa de Los Ferrocarriles del Estado. Santiago de Chile. Available at ⟨https://www.efe.cl/corporativo/documentos/memorias-anuales/efe-trenes-de-chile/⟩.
[80] Grupo-EFE (2015) Memoria Anual 2015 Empresa de Los Ferrocarriles del Estado. Santiago de Chile. Available at ⟨https://www.efe.cl/corporativo/documentos/memorias-anuales/efe-trenes-de-chile/⟩.
[81] Grupo-EFE (2016) Memoria Anual 2016 Empresa de Los Ferrocarriles del Estado. Santiago de Chile. Available at ⟨https://www.efe.cl/corporativo/documentos/memorias-anuales/efe-trenes-de-chile/⟩.
[82] Grupo-EFE (2017) Memoria Anual 2017 Empresa de Los Ferrocarriles del Estado. Santiago de Chile. Available at ⟨https://www.efe.cl/corporativo/documentos/memorias-anuales/efe-trenes-de-chile/⟩.
[83] Grupo-EFE (2018) Memoria Anual 2018 Empresa de Los Ferrocarriles del Estado. Santiago de Chile. Available at ⟨https://www.efe.cl/corporativo/documentos/memorias-anuales/efe-trenes-de-chile/⟩.
[84] Grupo-EFE (2019) Memoria Anual 2019 Empresa de Los Ferrocarriles del Estado. Santiago de Chile. Available at ⟨https://www.efe.cl/corporativo/documentos/memorias-anuales/efe-trenes-de-chile/⟩.
[85] EFE (2020) Reporte Integrado 2020 Empresa de Los Ferrocarriles del Estado. Santiago de Chile. Available at ⟨https://www.efe.cl/corporativo/documentos/memorias-anuales/efe-trenes-de-chile/⟩.
[86] EFE (2021) Reporte Integrado 2021 Empresa de Los Ferrocarriles del Estado. Santiago de Chile. Available at ⟨https://www.efe.cl/corporativo/documentos/memorias-anuales/efe-trenes-de-chile/⟩.
[87] Esteban, R. (2019). Formulación de una estrategia para aumentar el transporte de carga red EFE. Tesis de Magister. Universidad de Chile, Facultad de Ciencias Físicas y Matemáticas, Departamento de Ingeniería Industrial.
[88] Grupo-EFE. (2015). Bases Técnicas Licitación Pública Estudio de Ingeniería de Detalle – Puentes Zona Sur y Zona Norte 2ª Etapa.
[89] Hayward A. The Construction of Railway Bridges Then and Now. *The International Journal for the History of Engineering &*. Technology 2014;84(1):59–87.
[90] EFE. (1947). Ferrocarriles del Estado Chile. Departamento de Vía y Obras. Normas técnicas para el cálculo de puentes metálicos. Talleres Gráficos de los Ferrocarriles del Estado.
[91] Grupo-EFE. (2014). Plan Maestro de Puentes. Criterios de Diseño y Modelación. Empresa de Ferrocarriles del Estado.

[92] INN. (2005). *Norma Chilena NCh203–2005 Acero para uso estructural – Requisitos.* Instituto Nacional de Normalizacion.
[93] Larsson, T. (2009). Fatigue assessment of riveted bridges. Doctoral Dissertation, Lulea University of Technology, Lulea, Sweden.
[94] Höhler, S. (2005). *Material properties of Metal Railway Bridges.* Technical report, Sustainable Bridges. WP4-S-R- 001.
[95] MIDEPLAN-SECTRA. (2003). REDEFE: Recomendaciones de Diseño para Proyectos de Infraestructura Ferroviaria. Seccion 5. Obras de Arte. Santiago de Chile: Gobierno de Chile, Sectra.
[96] EFE. (2017). Compilation of structural drawings of Bridge A, including initial drawings from Le Creusot Company and all structural interventions made to the bridge.
[97] EFE. (1927). Structural drawings of floor system of Bridge A. Ferrocarriles del Estado. Departamento de la Via y Obras.
[98] EFE. (1935). Structural drawings of truss beams of Bridge A. Ferrocarriles del Estado. Departamento de la Via y Obras.
[99] EFE Trenes de Chile (2021). Reporte Integrado. Empresa de los Ferrocarriles del Estado.
[100] GlobalData. (2019, September 23). *Railway Technology*. Retrieved from Chile's government launches its biggest railway investment programme in history: ⟨https://www.railway-technology.com/comment/chiles-government-launches-its-biggest-railway-investment-programme-in-history/⟩.
[101] Thomson, I. and Angerstein, D. (2000) Historia del ferrocarril en Chile. Colección Sociedad y Cultura. Dirección de Bibliotecas, Archivos y Museos, Santiago de Chile.
[102] Coombs M. Chil Steam Locomot List Part 5 All locos List Build, Index Locat 2022; 51:v2.
[103] Coombs, M. (2022b). Chilean steam locomotive list. Part 1. Broad gauge locos, v2.51.
[104] Ferrocarriles de Estado de Chile (1886). Segunda memoria presentada al señor Ministro del Interior por el Director Jeneral de los Ferrocarriles del Estado correspondiente al año 1885. Valparaíso, Imprenta de "La Patria"
[105] Fepasa (2004). Memoria anual 2004 Ferrocarril del Pacifico S.A.
[106] Fepasa (2005). Memoria anual 2005 Ferrocarril del Pacifico S.A.
[107] Fepasa (2006). Memoria 2006 Fepasa-Ferrocarril del Pacifico S.A.
[108] Fepasa (2007). Memoria 2007 Fepasa-Ferrocarril del Pacifico S.A.
[109] Fepasa (2008). Memoria Anual 2008 Fepasa-Ferrocarril del Pacifico S.A.
[110] Fepasa (2010). Memoria Anual 2010 Fepasa-Ferrocarril del Pacifico S.A.
[111] Fepasa (2011). Memoria Anual 2011 Fepasa-Ferrocarril del Pacifico S.A.
[112] Fepasa (2012). Memoria Anual 2012 Fepasa-Soluciones en Transporte.
[113] Fepasa (2013). Memoria Anual 2013 Fepasa-Soluciones en Transporte.
[114] Fepasa (2014). Memoria Anual 2014 Fepasa-Soluciones en Transporte.
[115] Fepasa (2015). Memoria Anual 2015, Reporte Integrado. Fepasa-Soluciones en Transporte.
[116] Fepasa (2016). Memoria Anual 2016, Reporte Integrado. Fepasa-Soluciones en Transporte.
[117] Fepasa (2017). Memoria Anual 2017, Reporte Integrado. Fepasa-Soluciones en Transporte.
[118] Fepasa (2018). Memoria Anual 2018, Reporte Integrado. Fepasa-Soluciones en Transporte.
[119] Fepasa (2019). Memoria Anual 2019, Reporte Integrado. Fepasa-Soluciones en Transporte.
[120] Fepasa (2020). Memoria Anual 2020, Reporte Integrado. Fepasa-Soluciones en Transporte.
[121] Fepasa (2021). Memoria Anual 2021, Reporte Integrado. Fepasa-Soluciones en Transporte.
[122] Simms, W. (2001) The Railways of Chile. Volumen IV –Central Chile. West Sussex UK, Gadd's Printers.
[123] Simms, W. (2002) The Railways of Chile. Volumen V – Southern Chile. West Sussex UK, Gadd's Printers.
[124] Sommers, G.J. "SDL39's find a new home in Chile". Motive Power. 2008.
[125] Ferrocarriles del Estado (1984). Catálogo de vagones. Santiago de Chile.
[126] CSI (2019) "SAP2000 Integrated Software for Structural Analysis and Design". Computers and Structures Inc., Berkeley, California.
[127] Philbrick TW, Zodo GW, Schiff SD. Fatigue assessment of through plate girder railway bridges. J Struct Eng 1995;121(11):1613–9.
[128] Adasooriya ND, Pavlou D, Hemmingsen T. Fatigue strength degradation of corroded structural details: a formula for S-N curve. Fatigue Fract Eng Mater Struct 2020;43(4):721–33. https://doi.org/10.1111/ffe.13156.